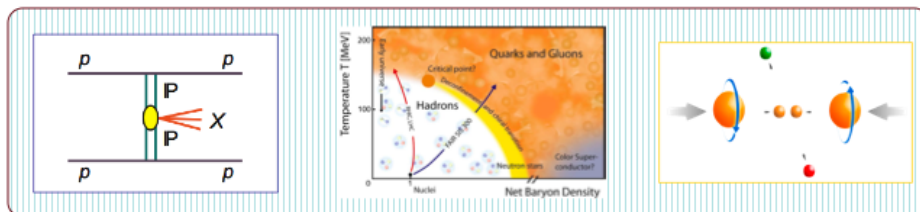
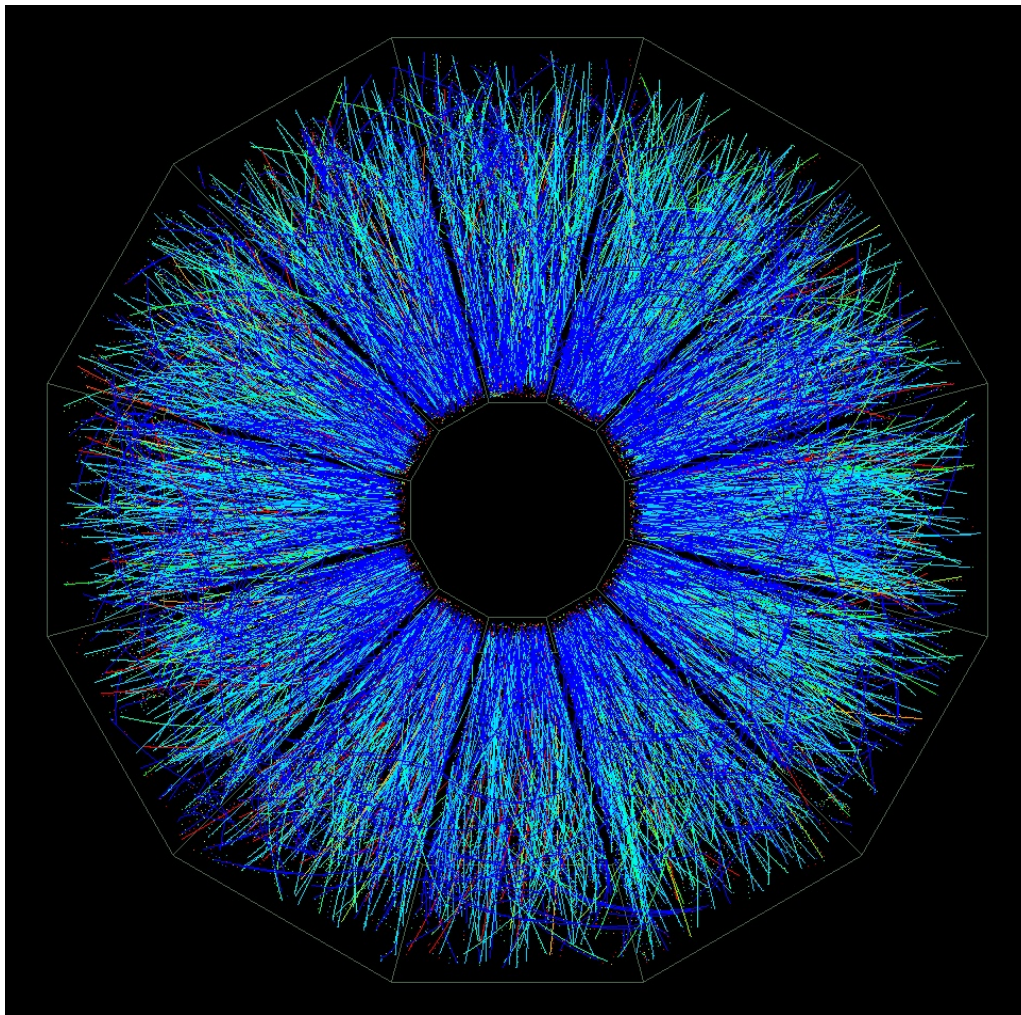


# RHIC Beam Use Request For Runs 14 and 15

The STAR Collaboration  
May 28, 2013



## Table of Contents

<b>1. Executive Summary</b> .....	<b>3</b>
<b>2. Report on Run 13 Performance</b> .....	<b>6</b>
<b>2.1 Summary of Run 13 polarized proton collisions</b> .....	<b>6</b>
<b>2.2 Status of the Forward GEM Tracker (GEM)</b> .....	<b>7</b>
<b>2.3 Status of the Heavy Flavor Tracker (HFT)</b> .....	<b>9</b>
<b>2.4 Status of the Muon Telescope Detector (MTD)</b> .....	<b>12</b>
<b>3. Study of the Properties of QGP at RHIC</b> .....	<b>13</b>
<b>3.1 Introduction</b> .....	<b>13</b>
<b>3.2 Previous results on heavy flavor hadron measurements</b> .....	<b>13</b>
<b>3.3 HFT physics goals and the beam use request</b> .....	<b>14</b>
<b>3.4 MTD physics goals and the beam use request</b> .....	<b>19</b>
<b>3.5 Gamma-jet measurement</b> .....	<b>24</b>
<b>3.6 Beam energy scan program</b> .....	<b>25</b>
<b>4. Study of p+p and p+A Collisions</b> .....	<b>30</b>
<b>4.1 Introduction</b> .....	<b>30</b>
<b>4.2 Recent highlights from the spin program</b> .....	<b>31</b>
<b>4.3 Run 15 request</b> .....	<b>37</b>
<b>4.4 Physics with 200 GeV longitudinally polarized p+p collisions</b> .....	<b>41</b>
<b>4.5 Physics with 200 GeV transversely polarized p+p collisions</b> .....	<b>42</b>
<b>4.6 Physics with transversely polarised p+A collisions</b> .....	<b>44</b>
<b>5. Physics with Tagged Forward Protons at STAR</b> .....	<b>55</b>
<b>5.1 Central exclusive production (CEP) in p+p collisions</b> .....	<b>55</b>
<b>5.2 Elastic scattering at medium <math> t </math></b> .....	<b>57</b>

RHIC Beam Use Request  
For Runs 14 and 15

*The STAR Collaboration*

May 28, 2013

## 1. Executive Summary

The STAR Collaboration makes the following two-year beam-use proposal, in order to achieve its spin and relativistic heavy ion physics goals on a timescale consistent with intense international interest and competition in these areas, as well as to utilize RHIC beams effectively, taking full advantage of planned improvements in machine and detector capability as a function of time:

Run	Energy	Time	System	Goal
14 <sup>(1)</sup>	$\sqrt{s_{NN}}=200\text{GeV}$	14-week	Au+Au	HFT & MTD heavy flavor measurements, $\mathcal{L}=10\text{ nb}^{-1}$ , 1000M M.B.
	$\sqrt{s_{NN}}=15\text{GeV}$	3-week	Au+Au	1) Collect 150M M.B. events for CP search 2) Fixed-target data taking <sup>(3)</sup>
15 <sup>(2)</sup>	$\sqrt{s_{NN}}=200\text{GeV}$	5-week	p+Au	Study saturation physics, pA-ridge and heavy ion reference, $\mathcal{L}=300\text{ nb}^{-1}$
	$\sqrt{s}=200\text{GeV}$	12-week	1) p+p	1) Heavy ion reference data $\mathcal{L}=90\text{ pb}^{-1}$ , 500M M.B.
			2) transverse 6 weeks	2) Study transversity, Sivers effects $\mathcal{L}=40\text{ pb}^{-1}$ , 60% pol.
3) longitudinal 6 weeks	3) Study $\Delta g(x)$ $\mathcal{L}=50\text{ pb}^{-1}$ , 60% pol.			

**Table 1-1: STAR Beam Use Request for Runs 14 and 15.**

- (1) 22 cryo-week, 5 weeks for overhead and initial commissioning of two species. Total of 17 weeks production with two species.
- (2) 22 cryo-week, 17 weeks production with two species.

(3) Fixed target data taking concurrently with the collider mode at 15 GeV.

In this proposed physics-driven plan, the STAR Collaboration intends to make the most efficient use of RHIC beam time and upgrades in order to make timely progress in determining the collectivity and energy loss of the heavy flavors in high-energy nuclear collisions as well as the gluon helicity distributions of the proton with the polarized proton-proton collisions.

The primary goals of the proposed program are:

**Run 14:** 22 cryo-week, 17 weeks for physics production at two colliding energies. STAR's priorities for Run 14 are:

- a) Fourteen weeks:  $\sqrt{s_{NN}} = 200$  GeV Au+Au collisions with the completed Heavy Flavor Tracker (HFT) and Muon Telescope Detector (MTD). This will be the first run in a multi-year program of precision measurements in the charm and bottom sector. The HFT will be used to directly reconstruct open charm hadrons, extracting the charm hadron collectivity and energy loss. The completed MTD will be used to measure quarkonium production in di-muon channels and extend e- $\mu$  correlations. At the beginning of the run, we will commission the full HFT along with other subsystems Intermediate Silicon Tracker (IST) and Silicon Strip Detector (SSD). Further running will be needed in subsequent years for measurements of the  $\mathcal{A}_C$ , and to extend the precision of the measurements of higher Upsilon states.
- b) Three weeks:  $\sqrt{s_{NN}} = 15$  GeV Au+Au collisions. In the RHIC Beam Energy Scan Phase-I (BES-I) program we have observed intriguing changes in several observables such as charged hadron nuclear modification factor  $R_{AA}$ , identified hadron anisotropic parameter  $v_2$ , and higher moments for net-protons at the colliding energy below 20 GeV. The 15 GeV results will fill the large gap between 19.6 GeV and 11.5 GeV.

In addition, STAR will take fixed-target data to examine Au+Au collisions at beam energy of 7.5 GeV ( $\sqrt{s_{NN}} = 4.0$  GeV) concurrently with the collider mode.

**Run 15:** 22 cryo-week, 17 weeks for physics production with two species. In this run STAR's priorities are:

- a) Twelve weeks:  $\sqrt{s} = 200$  GeV polarized p+p collisions, corresponding to  $90 \text{ pb}^{-1}$  integrated luminosity and 60% polarization with the luminosity upgrade compared to Run 12 afforded by the electron lenses. The run will be split in half between running with transverse and longitudinal polarization. We assume very conservatively that in the first 6 weeks (transverse) no luminosity gain of the e-lenses will be available. The physics for this part of the p+p run goals is to provide significant further constrain on observables sensitive to the transverse spin structure of the proton, i.e. transversity and the Sivers effect. Further new observables are  $A_N$  for exclusive  $J/\Psi$  production in ultra peripheral p+p collisions and  $A_N$  in diffractive production. The 2<sup>nd</sup> 6 weeks will be with

longitudinal polarization. We assume that the full luminosity gain due to the e-lenses can be realized. The data-set will provide further constrain of the gluon polarization through inclusive and di-jets at mid-rapidity, but will also allow to reach lower  $x$  by measuring  $A_{LL}$  for  $\pi^0$  in the forward meson spectrometer.

In addition, a goal of the pp-run is to accumulate a heavy ion reference data sample with the HFT and MTD. For the HFT, we estimate that this dataset will provide approximately 1/4 of the event count for precision heavy flavor measurements at STAR. Further running will be needed for precision measurements.

- b) Five weeks:  $\sqrt{s_{NN}} = 200$  GeV  $p^{\uparrow}+Au$  collisions to collect  $300 \text{ nb}^{-1}$ . The program will address questions as gluon saturation, cold nuclear effects on open heavy flavor and heavy quarkonia production, the study of the ridge in pA, the Cronin effect and strangeness enhancement in small-size systems. Utilizing the polarization of the proton the ratio of single spin asymmetries in  $\pi^0$  production at forward rapidity in p+p and p+A can be used to get a handle on the scale of the saturation. Further the asymmetry for exclusive  $J/\Psi$  production in UPC in p+A can be measured to get a first look on the generalized parton distribution function  $E$  for gluons.

## 2. Report on Run 13 Performance

### 2.1. Summary of Run 13 polarized proton collisions

During Run 13, we have collected data for 510 GeV longitudinally polarized p+p collisions with the STAR fully installed FGT (All 24 quadrants were installed for the run.). As we prepare for the Beam User Request, we are still collecting data for p+p collisions at  $\sqrt{s_{NN}} = 510$  GeV. At this point all of the STAR's goals for single and double spin measurements have been achieved.

From improvements to the STAR DAQ system and RCF capacity to analyze the data collected, STAR has to date collected a large dataset of approximately 1.542 petabytes in Run 13, increasing our overall dataset by 28% relative to all previous datasets combined, as shown in Figure 2.1-1.

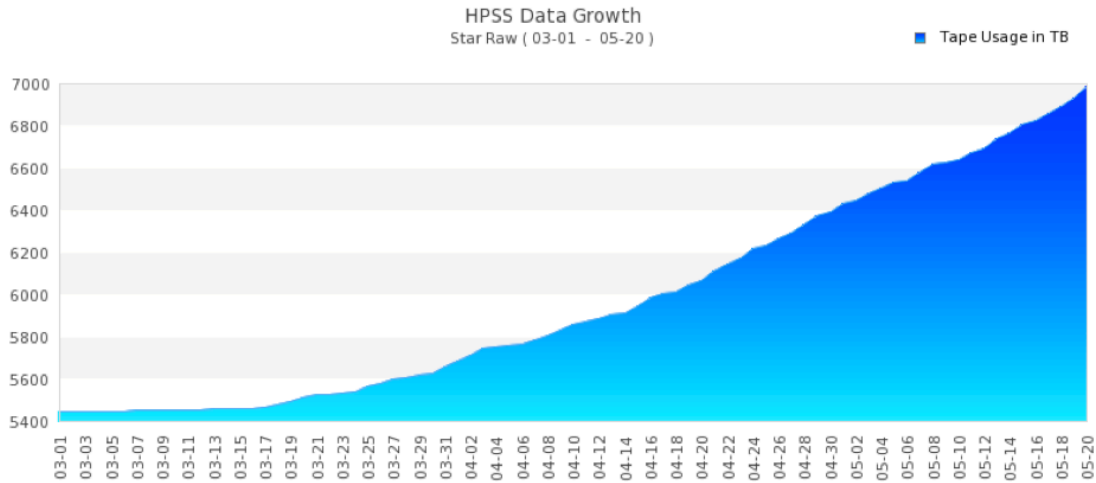


**Figure 2.1-1:** Integrated raw dataset size of STAR data, in Terabytes, over all years of STAR data taking. The plot begins at a baseline at the beginning of Run 13 and continues to May 20, 80% through the p+p run.

Polarized proton beams were collided at  $\sqrt{s} = 510$  GeV center-of-mass energies in Run 13. The proton spins were oriented for the entire run longitudinally. The luminosity and polarization goals were based on the projected RHIC performance from the BNL CAD ([www.rhichome.bnl.gov/RHIC/Runs/RhicProjections.pdf](http://www.rhichome.bnl.gov/RHIC/Runs/RhicProjections.pdf)) for Run 13, and assume a STAR sampling efficiency of 60%. The accelerator performed extremely well at the 2<sup>nd</sup> half of the 2013 run, delivering integrated luminosities near the maximum of the projected range, and meeting polarization goals with periods of ~60% polarization at 510 GeV. Figure 2.1-2 shows the yellow and blue beam polarization, as measured by the hydrogen jet target, versus fill for 510 GeV.

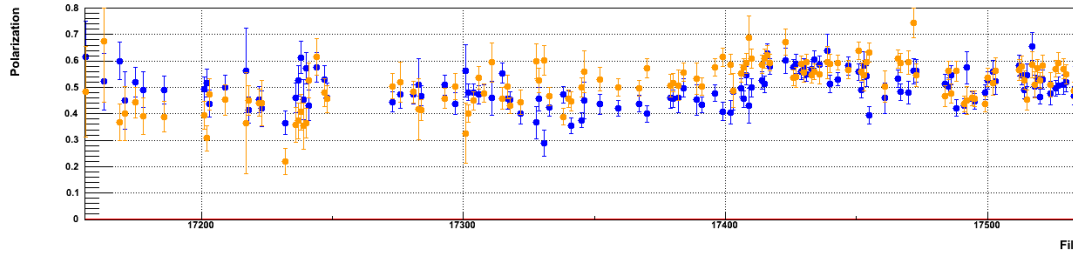


**Figure 2.1-2:** Blue and yellow beam polarization versus fill number, as measured by the hydrogen jet target. The plot includes fills till May 22<sup>nd</sup>.

**Physics results:** The total FOM for the  $\sqrt{s} = 510$  GeV longitudinal running period was significantly higher in Run 13 compared to the performance in Runs 9 to 12. STAR collected till May 22<sup>nd</sup> a dataset with FOMs of  $P^2L \sim 60 \text{ pb}^{-1}$  for the W single-spin analysis, and  $P^4L \sim 16 \text{ pb}^{-1}$  for the double-spin ( $A_{LL}$ ) jet, hadron, and photon measurements. This is nearly a factor of  $\sim 2.7$  improvement in FOM rate compared to what was achieved in Run 12.

To further improve the  $\Delta g(x)$  constraint and its integral, we plan to follow three steps in the upcoming years: (1) reduce the statistical and systematic uncertainties jets and di-jet  $A_{LL}$ . (2) Make use of correlation measurements such as di-jets, which give access to the partonic kinematics and thus the functional form of  $\Delta g(x)$ . The functional form of  $\Delta g(x)$  also provides insight in the dynamical origin of gluons inside the proton. First results from di-jets at STAR have been released for the 2009 run. (3) Access lower  $x$  by performing measurements at large forward rapidity utilizing the FMS.

## 2.2. Status of the Forward GEM Tracker (FGT)

During the summer 2012 shutdown, prior to Run 13, the FGT partial assembly of 14 quarter sections ('old quarter sections') was extracted for full completion. At the same time, an additional set of 14 quarter sections ('new quarter sections') were assembled at MIT Bates. Each of the 14 old quarter sections were transported to MIT Bates to test the leakage current and gain performance using a simple scope test procedure based on the signal induced by an  $^{55}\text{Fe}$  source which was only available for the FGT project at MIT Bates. The majority of all old quarter sections along with several *new* quarter sections were then tested in a cosmic-ray test stand at BNL prior to the full installation. First results on the cosmic-ray test data of residuals and efficiencies were obtained. The Run 12 Cu-Au data sample, the Run 13 p+p data sample, as well as the cosmic-ray test data, showed a consistent performance of the reconstructed residuals. The gas and pedestal performance was carefully tested prior to the full installation. The assembly, testing and installation of quarter sections prior to Run 13 proceeded in two phases. Phase I allowed the full installation of 16 quarter-sections mounted on disks 1-4 in September 2012. During phase II, the FGT installation was completed in November 2012. Figure 2.2-1 (left) shows a photograph of the West side of the STAR experiment showing the installation of disk 5-6 in November 2012. The full FGT installation in fall 2012 completed the FGT construction project.

Three quarter sections were disabled following the installation even though all quarter sections were successfully tested prior to the actual installation. A common gas line for both quarter section 4B and 4C was bent likely during the installation. In addition, excessive leakage current was observed for quarter section 6C. It was therefore decided to disable all three quarter sections prior to Run 13. The repair of the bent gas line and the replacement of quarter section 6C is planned for summer 2013.

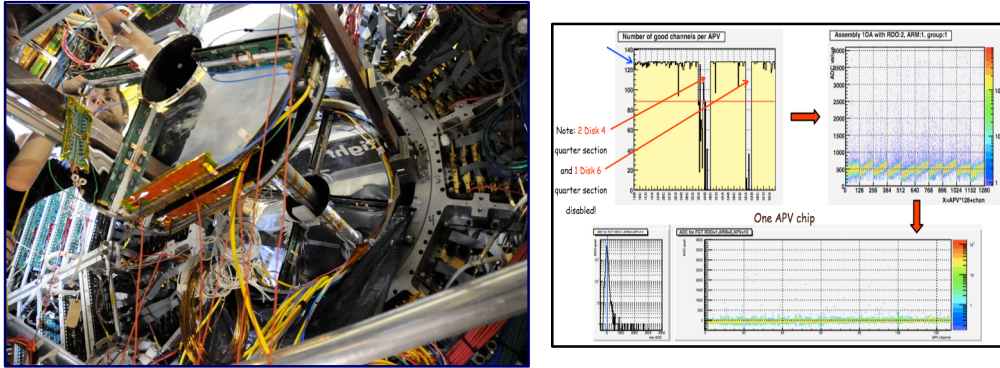


**Figure 2.2-1:** (Left) Photograph of the West side of the STAR experiment showing the installation of disk 5-6 in November 2012. (Right) FEE performance showing the number of good channels per APV chip (top left) along with the chip performance for one assembly with 10 APV chips (top right), one individual APV chip (bottom right) and the actual signal projection (bottom left).

Figure 2.2-1 (right) displays the FEE performance showing the number of good channels per APV chip (top left) along with the chip performance for one assembly with 10 APV chips (top right), one individual APV chip (bottom right) and the actual signal projection (bottom left). It should be noted as shown in Figure 2.2-1 that three quarter sections are disabled. The actual number of good channels is therefore reduced and amounts to roughly 70%. All quarter sections on disks 1/2 show overall a good performance whereas quarter sections on disks 3-6 suffer from various FEE issues related to the APV chip communication and programming.

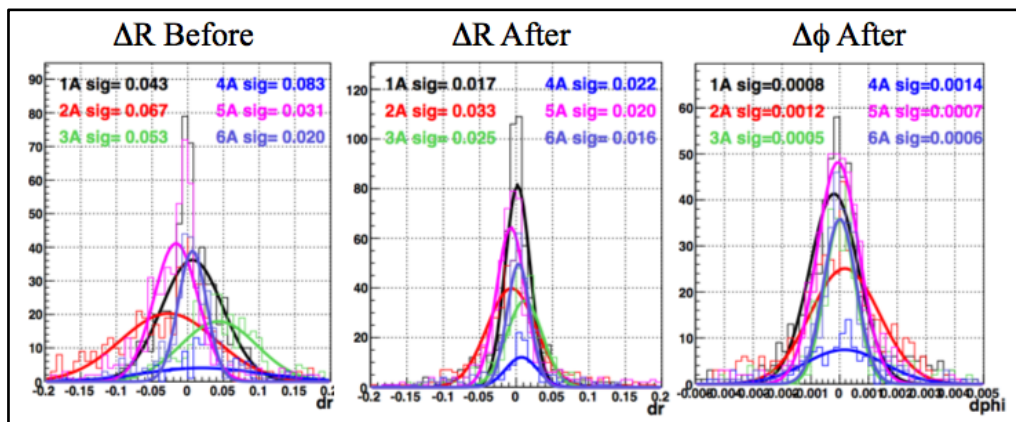


**Figure 2.2-2:** Residual distributions for all 'A' quarter sections for all six disks before and after alignment in R and after alignment in the azimuthal angle.

Figure 2.2-2 shows the residual distributions for all ‘A’ quarter sections for all six disks before and after alignment in R and after alignment in the azimuthal angle  $\phi$ . The preliminary evaluation is consistent with expectations.

The Run 13 performance can be summarized as follows:

- Satisfactory performance for all quarter sections on Disks 1 and 2 in terms of readout and actual detector behavior.
- 3 of the 24 quarter sections disabled: 2 due to gas line blockage during installation (Sections 4C and 4D) and 1 due to excessive leakage current (Section 6C)
- FEE: Issues largely with APV chip communication / programming for some of the chips, in particular on Disk 4.
- DAQ: Limitation of data taking rate ( $\sim 200$  Hz) with original control module (ARC-I). Upgrade with new ARC-II for Run 13.
- Residual distributions consistent with previous results in Cu-Au and cosmic-ray tests.

The current 510 GeV p+p data taking will continue until June 10, 2013, the requested Figure-of-Merit focusing on the W single-spin asymmetry measurement ( $P^2L$ ) of  $50\text{pb}^{-1}$  has been excited. The physics goal for Run 13 is a first measurement of the  $W^{+/-}$  asymmetries at backward / forward leptonic rapidity over one bin. Based on the analysis of the Run 13 data STAR will evaluate the need for future p+p 510 GeV runs to achieve the FGT physics goals.

### **2.3. Status of the Heavy Flavor Tracker (HFT)**

The HFT detector system is under construction, and it is scheduled to have the complete detector system ready for run 14 following installation in August-September 2013. The PXL sub-system is being commissioned in the engineering run as described below. The IST is nearing completion of all the detector components and initial assembly is scheduled to start in June 2013. The development of the SSD electronics is also proceeding well.

The HFT consists of 4 layers of silicon detectors grouped into three subsystems with different technologies, guaranteeing increasing resolution when tracking from the TPC towards the vertex of the collision. The Silicon Strip Detector (SSD) is an existing detector in double-sided strip technology. It forms the outermost layer of the HFT. The Intermediate Silicon Tracker (IST), consisting of a layer of single-sided strip-pixel detectors, is located inside the SSD. Two layers of silicon pixel detector (PXL) are inside the IST. The pixel detectors have the resolution necessary for a precision measurement of the displaced vertex. With the HFT, the Time-of-Flight detector, the

TPC, and the Barrel Electromagnetic Calorimeter STAR will study the physics of mid-rapidity charm and bottom production.

**Engineering Run:** All the supporting mechanical structures for the PXL subsystem has been fabricated and used to install 3 prototype PXL sectors covering 30% of the azimuthal angle. The installation was performed on May 8, 2013 and the commissioning tasks have begun.

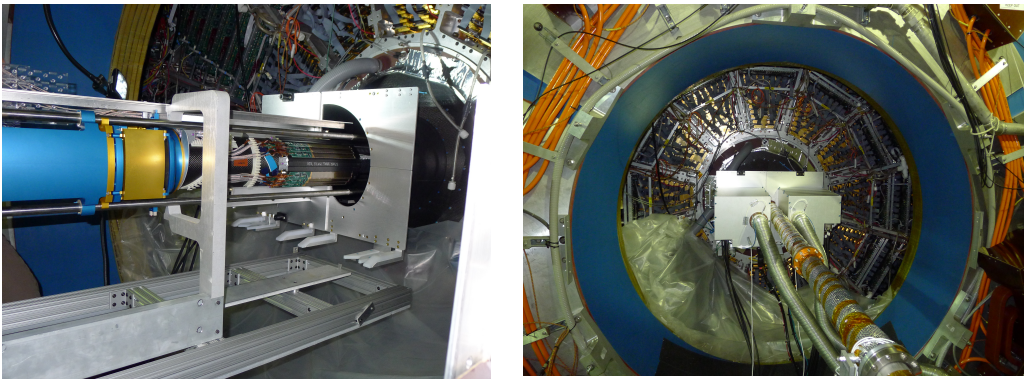


**Figure 2.3-1:** (Left) Second half of PXL detector with two instrumented sectors during installation. (Right) The installed PXL system as viewed from the East end of STAR. The mechanical and electric services, air hoses and cables, can be seen.

The engineering run with the HFT PXL detector serves a number of important functions that are required to finalize development of a robust detector system capable of producing useful physics in a timely fashion. Some functions address resolution of questions that could affect or require modification of the final design. Other functions address the need to get an early start on hardware and software commissioning in order to guarantee physics results from the first run with the HFT.

Some of the functions to be addressed in the ongoing run:

- Characterization of detector components, and determination of threshold and other settings
- Quantify Effects from beam condition on noise and hits in PXL instantaneous and over the course of the run. This includes latch-up and Single Event Upsets.
- Identify issue with trigger and DAQ.
- Investigate the track matching between TPC and PXL layer 1 and 2.
- Investigate vertex pointing quality
- Commissioning of calibration and analysis software

Some of these tasks are carried out in stand-alone mode though separate readout and control while other are done including the PXL system with the full STAR detector system. Since the ongoing run is 510 GeV p+p, it has been necessary to invoke dedicated shorter runs with reduced luminosity (by detuning the beam at STAR to a few percent of nominal luminosity) in order to reduce the pile-up of tracks in the TPC and triggering on high multiplicity events to allow for multiple tracks within the

reduced solid angle coverage. The environment is also very challenging due to the low-multiplicity to extract performance figures of merit. The installation and commissioning has already provided the HFT group with information on both mechanical as well as electronics, that will be used to improve the detector system for the final production, that has just started.

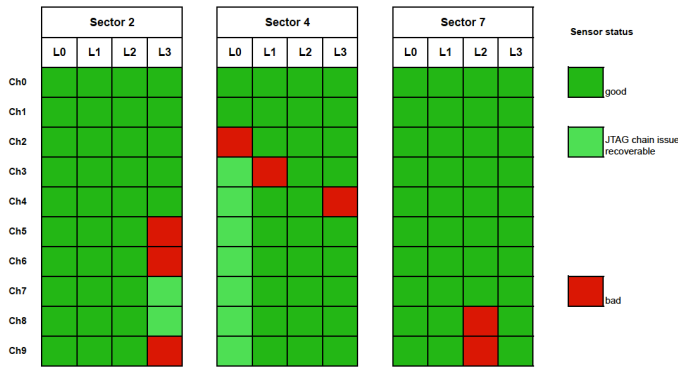


**Figure 2.3-2** Map of active sensors on the 3 ladders in the engineering run configuration. The dark green boxes are fully functioning, the light green are temporarily lost due to a JTAG issue and the red are lost.

A first low luminosity run was taken and has been analyzed. The PXL firmware is still in development, and the threshold settings have not been optimized so the sensors were somewhat noisy. The installed sectors have most sensors working. Figure 2.3-3 shows the map of working sensors in the engineering run configuration. One outer ladder was really quiet and an analysis looked at projections of the tracks to the TPC on the sensors and compared with sensor hits. The plot below, Figure 2.3-3, shows the deviation between track projections and hits in sensors on an outer ladder. The plots show the expected deviation due track resolution, shows that efficiency for picking the right hits is quite high, and that the initial analysis chain is under control. The results are promising The last weeks of the Run 13 will be used for further commissioning and to collect a larger low-luminosity data set to further evaluate response.

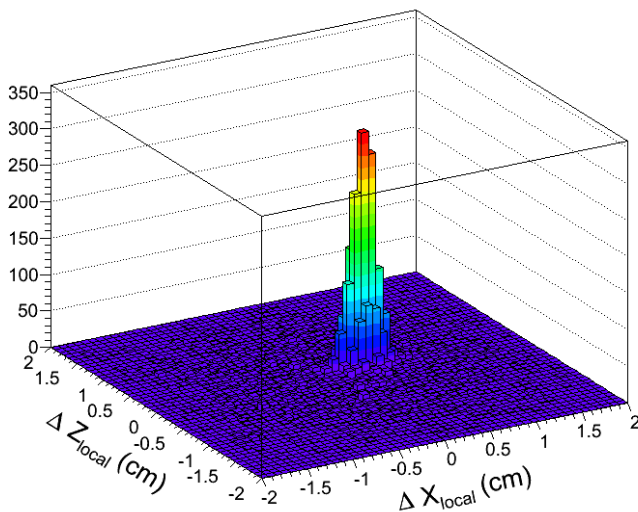


**Figure 2.3-3** 2D residuals in local coordinates on sensors on one ladder between projected TPC tracks onto the surface of sensors and hits on sensor, summed over all active sensors on that ladder. The resolution is that expected from the TPC track projection.

## 2.4. Status of the Muon Telescope Detector (MTD)

The design of the MTD was completed in May 2011. The five-gap module MRPC was selected for mass production. At the time we prepare for the BUR document, more than 60% MTD have been made and installed in STAR experiment. Since February 2013, the installed MTD has been running reliably and taking data smoothly.

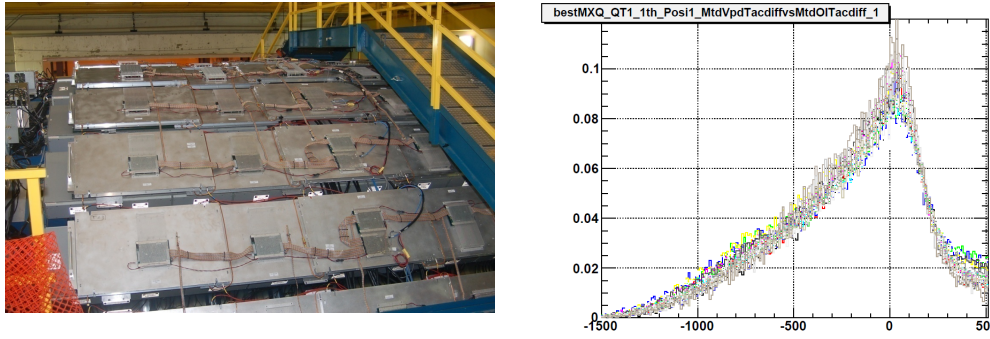


**Figure 2.4-1:** (Left plot) Top view of STAR detector with MTD modules covering 63% of the backlegs for run13. (Right plot) Alignment of online muon timing from all channels (20ps/ch) in trigger electronics from run13 p+p collisions.

Trigger commissioning aspects: In 2012 run the MTD took electron-muon and di-muon triggered events successfully. In order to sample the full luminosity of 200 GeV Au+Au collisions with limited bandwidth allowed for the MTD system in run 14, we need be able to cut on the trigger timing window within 1 nanosecond. This requires good trigger timing resolution. Therefore, we made a request for the change on the trigger algorithm in order to be able to do the timing correction at L0, namely, do the hit position and slewing corrections. On May 9th, 2013, the MTD trigger algorithm was ready and we successfully commissioned the MTD triggers on May 10th. Position correction was applied online. The dimuon and electron-muon triggers have been running smoothly since then. In addition, we have studied that with slewing correction, we can obtain 400 ps timing resolution for the trigger. This, together with further offline study, will help optimize the MTD trigger algorithm implementation in 200 GeV Au+Au collisions in Run 14.

## 3. Study of the Properties of QGP at RHIC

### 3.1. Introduction

One of the main focuses of the heavy ion programs at RHIC and LHC in the next decade is to quantify the properties of the strongly-coupled Quark-Gluon Plasma (sQGP) matter created in high energy heavy ion collisions. Heavy quarks represent as excellent probes for these investigations.

Compared to light quarks, heavy quarks have much higher intrinsic quark masses and their masses are not expected to be modified by the surrounding QCD medium. They are predominantly created via the initial hard scatterings, particularly at RHIC energies. The collective behavior of heavy quarks in the hydrodynamic region offers a direct experimental probe of the medium's thermalization at an early stage when the partonic sQGP medium is created. Due to their intrinsic large masses, various model calculations show that the production of heavy quarks at low  $p_T$  is more sensitive to the medium transport properties, shear viscosity per entropy  $\eta/s$ , for example, compared to light quarks. A complete understanding of the parton energy loss mechanism in the sQGP medium requires a systematic investigation of the mass (flavor) dependence of the particle yield suppression. Heavy quark production offers unique opportunities in all these directions. Measuring the heavy quark production spectra and correlations at RHIC is a DOE milestone in 2016.

### 3.2. Previous results on heavy flavor hadron measurements

Heavy flavor measurements have been pursued by PHENIX and STAR at RHIC for many years. One of the most striking observations was that heavy flavor decay electrons show a similar significant suppression in central Au+Au collisions as light flavor hadrons, shown in Figure 3.2-1 left plot [1]. This challenged the understanding of parton energy loss in the radiative loss framework, in which heavy quarks should lose less energy than light quarks due to the kinematic suppression of radiated gluons [2]. Several recent model calculations including the collisional energy loss mechanism can generally reproduce this suppression level [3]. However, the physics interpretation is complicated by decay kinematics and unknown charmed and bottomed hadron contributions to the measured electrons.

With the unprecedented statistics in the data collected in year 2009-2011 and the completion of the Time-Of-Flight (TOF) system, we were able to first measure the  $p_T$  spectra of  $D^0$  meson via hadronic decays even without the secondary vertex reconstruction. Figure 1 right plot shows the  $D^0 R_{AA}$  vs.  $p_T$  in central and minimum bias Au+Au collisions [4]. At  $p_T > 3$  GeV/c,  $D^0 R_{AA}$  is strongly suppressed while at 1-3

GeV/c, the data points show a modified hump structure, which may indicate strong interactions between charm quarks and the medium. The measurement has large uncertainties, which prevent us from drawing quantitative conclusions. Furthermore, with the current detector setup, it is almost impossible to make a meaningful measurement of the  $D^0 v_2$ , which is expected to carry cleaner information about the partonic medium thermalization.

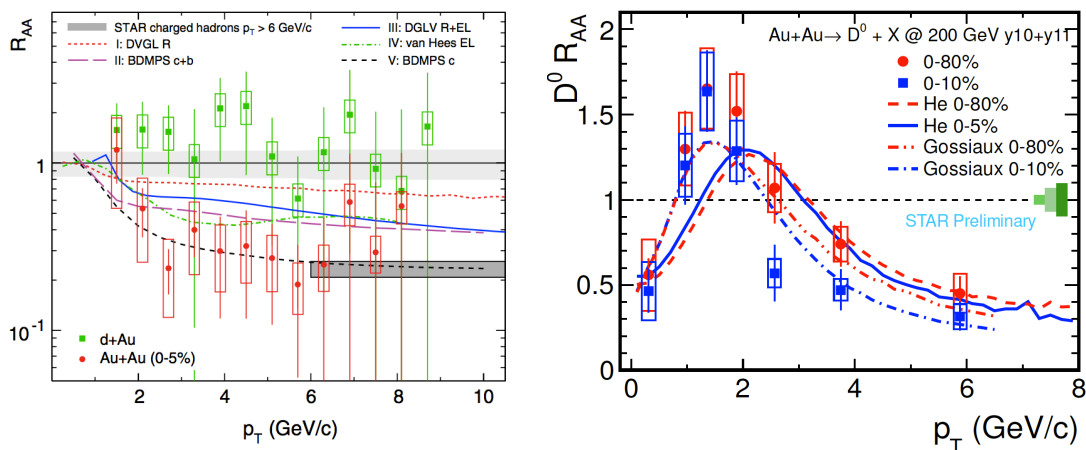


**Figure 3.2-1:** (Left) Nuclear modification factor  $R_{AA}$  of heavy flavor decay electrons in d+Au (green) and central Au+Au (red) collisions at  $\sqrt{s_{NN}} = 200$  GeV. (Right)  $R_{AA}$  of  $D^0$  mesons from central (filled squares) and minimum bias (filled circles)  $\sqrt{s_{NN}} = 200$  GeV Au+Au collisions.

### 3.3. HFT physics goals and the beam use request

**3.3.1 HFT physics goals:** Heavy Flavor Tracker (HFT) will allow precision measurements of open heavy flavor production and correlations in p+p and heavy ion collisions [5]. The HFT utilizes state-of-art thin silicon active pixel and silicon pad technology in order to topologically reconstruct the secondary decay vertices of open charmed and bottomed hadrons in high luminosity and high track density environment. The fine pixel array provides ultimate single hit resolution and the thin material design allows high tracking efficiency even for very low momentum tracks. The design goal is to have the track pointing resolution to the collision vertex to be better than 50  $\mu\text{m}$  for charged kaons with  $p_T \sim 800$  MeV (mean  $p_T$  of kaons from  $D^0$  decays).

The full HFT system covers full  $2\pi$  in azimuth and -1 to 1 in pseudo-rapidity. It perfectly matches the acceptance of mid-rapidity tracking and particle identification detectors – TPC, TOF, BEMC, which offers a great opportunity to make precision measurements on both single particle production and multi-fold particle correlations. The readout speed for all subsystems of HFT is compatible with the TPC rate, and thus can maximize the use of the RHIC-II luminosity.

The compelling physics program and associated measurements with the HFT are described below:

- 1) Total charm production cross section: This is the first critical test to establish that charm quarks are produced from initial hard scatterings and they are excellent probes for the medium properties at an early stage. Furthermore, precise knowledge of the total charm cross section is also essential to understand the mechanism of charmonium production at RHIC. The charm production rate is high enough so that charmonium production via the coalescence process is important. Precision determination of the total charm production cross section requires accurate measurements of various charmed hadron ( $D^0$ ,  $D^+$ ,  $D_s$ ,  $\Lambda_c$ ) spectra covering a wide  $p_T$  range at mid-rapidity from p+p to central A+A collisions. The measurement of  $\Lambda_c$  yields becomes critical in central heavy ion collisions because of the possible baryon enhancement over mesons in analogy to light hadrons.
- 2) Parton energy loss in the sQGP medium: The heavy flavor decay electron  $R_{AA}$  shows significant suppression in central Au+Au collisions. However, one big uncertainty in interpreting the data is the unknown relative contributions from various charmed and bottomed hadrons. In order to approach a complete understanding of the parton energy loss mechanism in the sQGP medium, one has to measure the hadron nuclear modification factors containing different flavors separately. The flavor dependent  $R_{AA}$  measurement, in particular, the double ratio of  $R_{AA}(b)$  over  $R_{AA}(c)$  has been proposed to disentangle two fundamental theory approaches - pQCD versus AdS/CFT in describing the parton energy loss in the medium [6]. HFT will enable precision measurements of  $R_{AA}$  of various charmed hadrons with a large dynamics range in  $p_T$ . This is the cleanest experimental approach yet to address the charm quark energy loss in heavy ion collisions. Heavy flavor decay electron channel will continue to serve as a complementary measurement, and HFT will enable the separation of charm and bottom decay electrons with controlled systematic accuracy benefiting from measurements of direct charmed hadrons.
- 3) Medium thermalization and transport properties: Heavy quarks interact with the medium differently compared to light quarks due to their large mass. Heavy quark collectivity has been proposed to be a direct experimental test to the thermalization of the partonic sQGP medium [7]. Furthermore, the heavy quark production shows great sensitivity to the drag coefficient that is connected to the medium transport properties (e.g.  $\eta/s$ ) [8]. The relevant kinematic region for these investigations is at low  $p_T$  where hydrodynamics is expected to dominate. One of the uniqueness of the HFT detector is the low mass design which allows precision charm hadron measurements down to as low as 0.5 GeV/c in  $p_T$ . Measurement of the charm hadron elliptic flow in the low  $p_T$  region will be directly used to address the medium thermalization issue. Large and uniform acceptance also offers a great opportunity to measure the charm quark correlations, which will be another complementary approach to investigate the medium thermalization and transport properties [9].

- 4) Charm chemistry / charm baryon production: RHIC experiments have observed a large baryon/meson enhancement in central Au+Au collisions compared to p+p collisions. One possible explanation is the coalescence production mechanism in the intermediate  $p_T$  region. It will be interesting to find out how the baryon-to-meson ratio looks like in the charm sector in direct analogy to the light hadrons. The yield of charm baryons is also important to determine the total charm yield, as well as to understand the charm decay electron  $R_{AA}$  in heavy ion collisions [10]. The high pixel resolution and the thin detector design allow measuring various charm hadron states, including  $\Lambda_c$  hadrons (challenging due to shorter decay lifetime) in all collision systems with good precision. This enables the determination of a possible  $\Lambda_c/D^0$  enhancement in central heavy ion collisions.

To achieve these goals, a multi-year three-stage run plan has been developed in STAR BUR proposal:

**Stage-I:** Au+Au run to measure the charm hadron  $v_2$  and  $R_{CP}$  in order to address the medium thermalization and parton energy loss.

**Stage-II:** p+p run to provide a baseline reference for  $R_{AA}$  and many other quantities in heavy ion collisions.

**Stage-III:** long Au+Au run(s) to measure charm baryons, bottom decay electrons and charm correlations in order to systematically investigate the sQGP medium properties.

**3.3.2 Beam Use Request for Run14 and 15:** The full HFT system will be installed and ready for physics before the Run14 starts. We make the requests for Run14 and Run15 to complete the first two stages.

**3.3.2.1 HI run request:** In Run 14, the primary goal of the stage-I Au+Au run is to make first measurements of charm hadron  $v_2$  and  $R_{CP}$ . Figure 3.3-1 left plot shows the projected statistical uncertainties for  $D^0$  meson  $v_2$  with 1 billion minimum bias events within the vertex region of  $|V_z| < 5\text{cm}$ . The projected uncertainties include the full tracking, PID and topological cut efficiencies. The online vertex z-position is selected via the timing difference between the east and west VPDs at STAR. The resolution of online  $V_z$  is about 5 cm in mid-central to central Au+Au collisions and decreases to about 10cm in peripheral collisions. With an online  $|V_z| < 5\text{cm}$  cut, about half of the selected events have the real  $V_z$  within  $|V_z| < 5\text{cm}$ . Thus, to accumulate 1B minimum bias events within  $|V_z| < 5\text{cm}$ , we need to trigger about 2B events, which can be collected in approximately 1400 DAQ hours or 14 weeks assuming 50% uptime at a recording rate of 500 Hz or higher.

With the same dataset, the binary-scaled ratio of central to peripheral spectra,  $R_{CP}$ , for directly reconstructed  $D^0$  mesons can be measured out to  $p_T \sim 10$  GeV/c with about 50% uncertainty. Measuring  $R_{AA}$ , rather than  $R_{CP}$ , requires large un-triggered and triggered datasets in p+p collisions at 200 GeV that will be discussed in the following subsection. Besides  $D^0$ , the requested data set will also allow the direct reconstruction of various other charmed hadrons, such as  $D^{+/-}$ ,  $D_s^{+/-}$ ,  $D^*$ , and  $\Lambda_c$ .

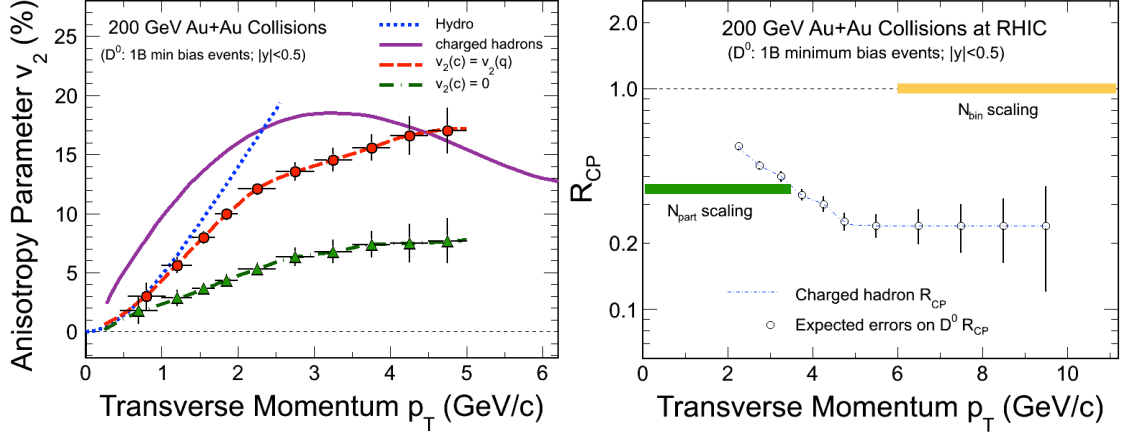


**Figure 3.3-1:** (Left) Projected statistical uncertainties for  $D^0$  meson  $v_2$  in 1B minimum bias collisions from two different model calculations. Also plotted are the prediction from an ideal hydrodynamic model and the measured charged hadron  $v_2$ . (Right) Projected statistical uncertainties for  $D^0$  nuclear modification factor  $R_{CP}$  in 1B minimum bias collisions assuming the same  $R_{CP}$  value as light hadrons.

Figure 3.3-2 left plot shows the projected errors for  $R_{CP}$  of electrons from charm and bottom decay electrons using the impact parameter method with minimum bias and High Tower (HT) triggered data sets. The central values are taken from a transport model calculation [11]. The  $1 \text{ nb}^{-1}$  recorded luminosity within  $|V_z| < 5 \text{ cm}$  will need 14 week Au+Au beam time considering the average CAD luminosity projection and 60% sampling efficiency (achieved in Run11 Au+Au 200 GeV). The luminosity fraction falling into  $|V_z| < 5 \text{ cm}$  was about 10% in Run 11, and it is expected to be improved to 13-15% with the new 56MHz RF system upgrade. The right plot of Figure 3.3-2 shows the projected errors on the bottom decay electron  $v_2$  from 1B minimum bias data set.

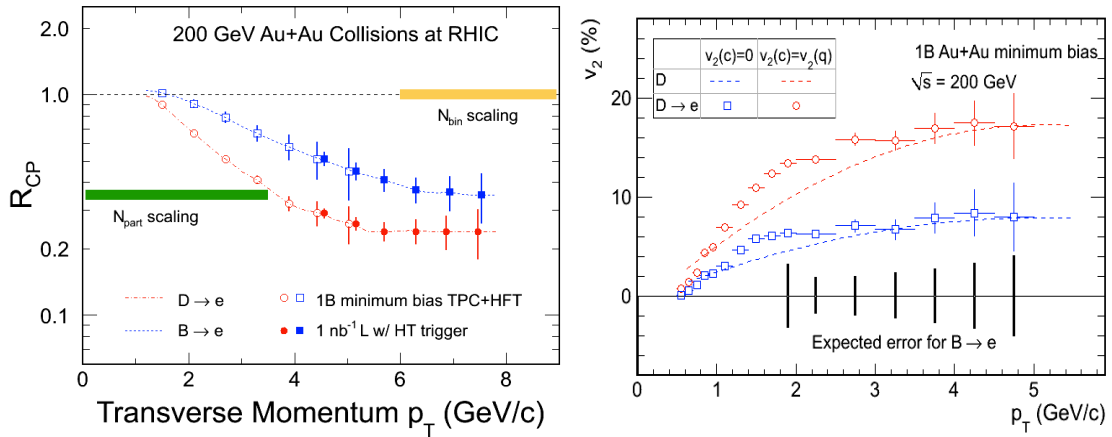


**Figure 3.3-2:** (Left) Projected statistical uncertainties for the  $R_{CP}$  of electrons from charm and bottom decays separately with HFT. The estimate is based on 1B minimum bias event sample plus  $1 \text{ nb}^{-1}$  sampled luminosity with HT triggers collected within  $|V_z| < 5 \text{ cm}$ . (Right) Projected statistical uncertainties for charm and bottom decay electron  $v_2$  with 1B minimum bias events.

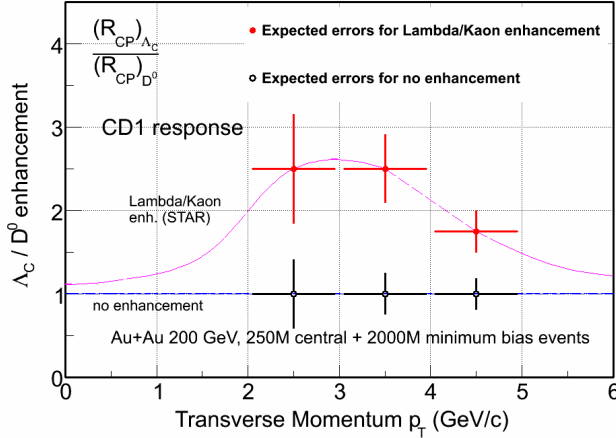


**Figure 3.3-3:** Projected statistical uncertainties on the  $\Lambda_c/D^0$  ratios with 250M central and 2B minimum bias events.

We request at least 250M 0-10% central triggered events within  $|V_z| < 5\text{cm}$  to improve the statistics in central Au+Au collisions for more precise RAA calculation, and to investigate high harmonic flows of D-mesons in central collisions. Furthermore, this will also allow the first measurement of the  $\Lambda_c/D^0$  ratio in central Au+Au collisions. Due to the finite online vertex resolution, to record this central data set we need to trigger roughly 500M 0-10% events with the online  $|V_z| < 5\text{ cm}$  cut. The factor of two data is needed (in the future, stage-III) in order to determine whether there is an enhancement in the  $\Lambda_c/D^0$  in central collisions compared to that of in peripheral collisions. Figure 3.3-3 shows the projected statistical uncertainties on the  $\Lambda_c/D^0$  ratios with 250M central and 2B minimum bias events.

**3.3.2.2 p+p run request for heavy ion reference data:** The 200 GeV p+p beam request is to set the baseline reference for heavy ion measurements, particularly driven by the precision for the  $D^0$   $R_{AA}$  measurements. We will make use of both untriggered data (minimum bias triggers) for precision  $D^0$  spectrum measurement at low  $p_T$  and triggered data to extend the  $p_T$  reach up to  $\sim 10\text{ GeV}/c$ . Therefore we request 500M p+p minimum bias events with  $|V_z| < 5\text{ cm}$  to allow a first  $R_{AA}$  assessment with reasonable precision. To record this data set needs about a 12-week beam time with 500Hz DAQ rate and 50% uptime. In order to reach comparable precision at low  $p_T$  region as in Au+Au collisions requested above, we need about 2B minimum bias p+p events which will require multiple years of 200 GeV p+p collisions.

The precision of high  $p_T$  heavy flavor hadron spectra can be improved by utilizing the EMCal higher tower (HT) triggered data set to trigger on one hadron leg and to sample the full luminosity. HT triggered data has been successfully used to measure the high  $p_T$   $K_S$  and  $\Lambda$  yield in p+p collisions to improve the baseline precision for  $R_{AA}$  calculations [12]. Figure 3.5 left plot shows the trigger efficiency for charged pions with two different HT thresholds from 200 GeV p+p in Run 6. This has been vetted using large minimum bias sample data. We will apply the same technique to measure the D-meson production with triggering on one charged daughter leg. At high  $p_T$ , the combinatorial background in the D-meson reconstruction in p+p collisions is small. To maximize the sampled luminosity, we will not be constrained by the HFT acceptance for this measurement. In a 12-week p+p 200 GeV run in Run15, the total sampled luminosity within  $|V_z| < 30\text{cm}$  with affordable bandwidth rate (BHT0\*VPDMB with no prescale)

and also considering the VPD minimum bias triggering efficiency and the vertex selection fraction is about  $8 \text{ pb}^{-1}$ . Figure 3.3-4 right plot shows relative errors of  $D^0$  raw yields reconstructed in 100M 0-10% central Au+Au events, 500M p+p MB events and  $8 \text{ pb}^{-1}$  sampled luminosity events in p+p with HT0 triggers. The triggered sample from p+p collisions will allow a comparable precision as central Au+Au collisions up to 10 GeV/c.

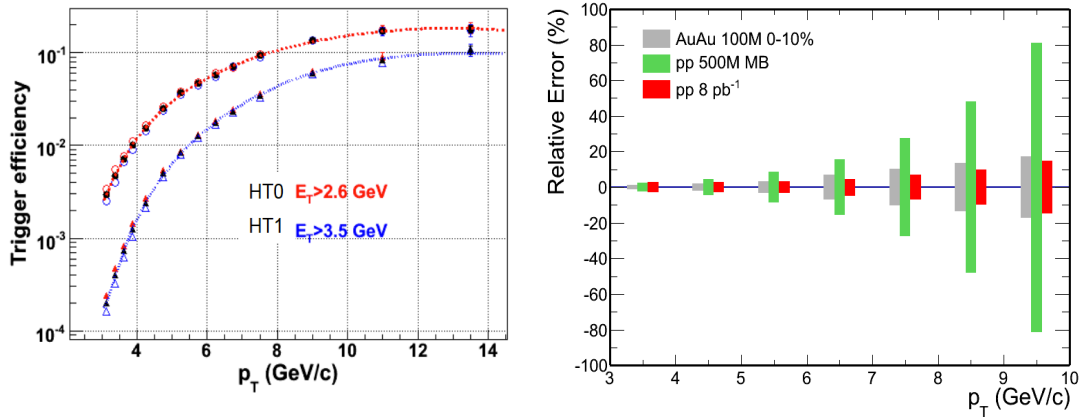


**Figure 3.3-4:** (Left) Barrel EMC trigger efficiency for charged pions with two different HT thresholds obtained from 2006 analysis [11]. (Right) Projected relative statistical uncertainties for 100M 0-10% central Au+Au events, 500M p+p minimum bias events, and  $8 \text{ pb}^{-1}$  sampled luminosity events with the HT0 ( $E_T > 2.6 \text{ GeV}$ ) trigger.

### 3.4. MTD physics goals and the beam use request

**3.4.1 Introduction:** STAR constructing a large-area and cost-effective Muon Telescope Detector (MTD) at mid-rapidity that will be completed for Run 14. The Time-of-Flight system it utilizes is based on multi-gap resistive plate chambers with precise timing and hit position. The technology and method are different from the conventional muon detector, consisting of a sandwich of tracking stations, trigger detectors, and absorbers, in high-energy particle and nuclear physics experiments. Among many exciting perspectives, we will be able to collect a large sample of  $J/\psi$  events for spectra and elliptic flow measurements (Figure 3.4-1 left plot), to separate different Upsilon states (Figure 3.4-1 right plot) with a clear advantage over electron decay channels due to the reduced Bremsstrahlung radiation and Dalitz decay background, and to provide a unique measurement of  $\mu-e$  correlations from heavy-flavor decays.

The open charm production rate is high enough at RHIC that the coalescence process becomes relevant for charmonium production. Knowledge of the total production cross-section for charm quarks is also essential as a baseline for  $J/\psi$  measurements. From a precise measurement of the spectra and the production ratios of charm hadron states, we will be able to extrapolate to the total yield for charm quark production. A unique

advantage of STAR due to its full azimuthal coverage is the detailed studies of charm-charm correlations. The angular correlation will be modified in heavy ion collisions due to the interactions between the heavy quarks and the medium. Measurements of the direct D-Dbar and e- $\mu$  correlations are sensitive to the effect of ‘partonic wind’ on charm quark correlations in high-energy nuclear collisions and the thermalization in high-energy nuclear collisions. Meanwhile, the semi-leptonic decays of heavy-flavor pairs are important component of dilepton spectra. Only such correlation measurements can provide experimental tool to separate QGP thermal radiation from the heavy-flavor decays in the dilepton spectra.

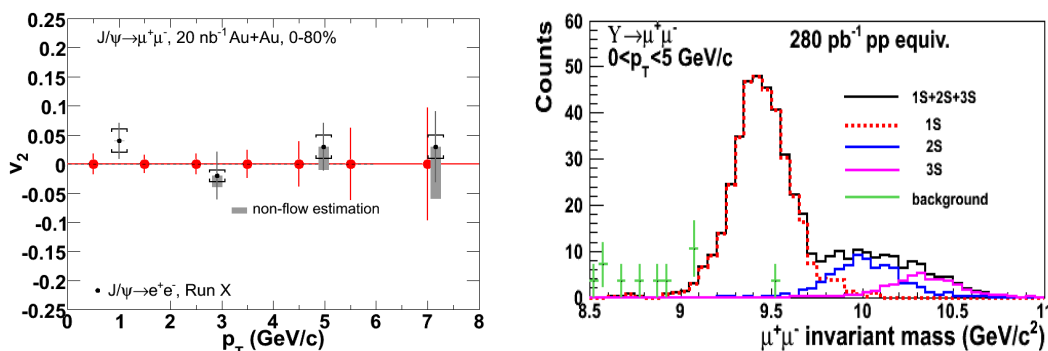


**Figure 3.4-1:** (Left) Projection of  $J/\psi$  (from muon pairs)  $v_2$  measurement from MTD. Data with error bars are from [13]. (Right) Projected Upsilon line-shapes of the 1S, 2S and 3S states and backgrounds measured in the MTD from  $280 \text{ pb}^{-1}$  Au+Au collisions at RHIC.

Measurements of the in-medium dissociation probability of the different quarkonium states are expected to provide an estimate of the initial temperature of the system. Dissociation of quarkonium in a thermal QCD system would ultimately provide evidence of color screening and free quarks. The  $J/\psi(1S)$  is the lightest and most abundantly produced quarkonium state accessible in experiment. However, significant decay contributions from excited states and the final state production via coalescence complicate the situation.  $\Upsilon(1S, 2S, 3S)$  states provide a natural thermometer since they are bottomia of three consecutive states. The ground state has a binding energy of 1.1 GeV and is way above the temperature reached at RHIC. However, the 2S and 3S states have binding energy at 0.54 and 0.2 GeV, respectively, and can be dissolved at RHIC. MTD provides the measurements allowing separate these three states at RHIC through the di-muon channel. The separation is made possible by MTD with reduced Bremsstrahlung radiation and enhanced trigger capability. Comparison of low- $p_T$   $J/\psi$  and  $\Upsilon$  yields at RHIC and LHC and study of the  $J/\psi$  azimuthal anisotropy could quantitatively further constrain the model interpretation. These requirements call for a comprehensive experimental quarkonium program at RHIC. The combined measurements by HFT and MTD from STAR offer a unique and comprehensive heavy flavor program to explore these exciting physics opportunities.

A transition to a different state is not only characterized by the increase of temperature, but also by the changes of degree of freedom and symmetries. The long-sought

signature of such a transition is chiral symmetry restoration. The experimental procedure of detecting signature related to the restoration is to study the in-medium dilepton decay of vector mesons. The spectral function from the remnant hadronic structure should transit to a smooth spectrum of QGP thermal radiation with increasing temperature and density. Great progress has been made in the last decade at SPS and RHIC. It has been experimentally demonstrated that the hadronic spectral function has been greatly modified in the medium. However, a quantitative assessment of its temperature dependence is absent. This requires consistency between thermal radiation at high temperature (dominant at RHIC) and modified hadronic decay (dominant at SPS) close to the phase transition. At RHIC energies and above, such dilepton measurements are hindered by the dominant “irreducible” background from semileptonic decay of open heavy-flavor pairs. STAR has demonstrated its unique capability of di-electron measurement with the combination of large-coverage TPC, EMC and TOF. With HFT and MTD upgrades, contribution to the dilepton spectra from the open heavy-flavor pair correlation is measurable with D-Dbar and e- $\mu$  correlation measurements all at mid-rapidity.

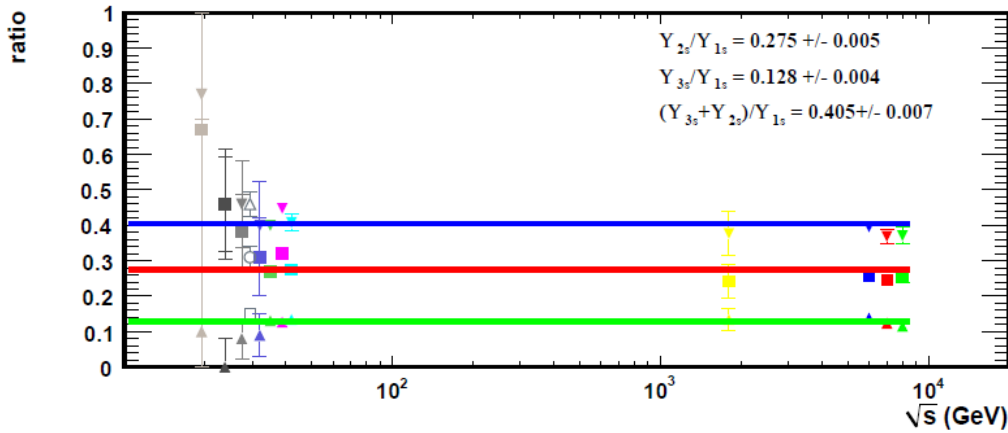


**Figure 3.4-2:** Collision energy dependence of the yield ratio of Upsilon states in p+p, p+pbar and p+A collisions.

**3.4.2: Run 14 requests:** Run 14 begins the physics program with the full MTD. The primary focus of this MTD run is on Quarkonia at RHIC energies, using muons to remove the issue of Bremsstrahlung tails in their line-shapes. This is most important in the separation of the Upsilon 1S from the (2S, 3S) states, all three of which are expected to be suppressed differently in the QGP. Figure 3.4-1 shows a projected line-shape with the MTD, showing that the 1S can be clearly separated from the 2S+3S, while the 2S and 3S can be separated statistically assuming a large statistics sample and good control over the line-shape. These measurements require a large integrated luminosity driven by the requirement in p+p reference data. Table 3.4-1 shows an estimate for the required luminosity for measurements of the 2S+3S and the 3S separately. We have investigated an alternative approach in obtaining the reference. Many experiments have measured the Upsilon yields and ratios of the three states. We have collected all the experimental results and survey the ratios of  $Y(2S)/Y(1S)$ ,  $Y(3S)/Y(1S)$  and  $Y(2S+3S)/Y(1S)$ . Figure 3.4-2 shows the results as a function of beam

energy for all the p+p, p+pbar and p+A results. The ratios are shown to be independent of beam energy with the world average value of  $\Upsilon(2S)/\Upsilon(1S)=0.275\pm 0.005$ ,  $\Upsilon(3S)/\Upsilon(1S)=0.128\pm 0.004$  and  $\Upsilon(2S+3S)/\Upsilon(1S)=0.405\pm 0.007$  when  $\sqrt{s} > 30$  GeV. Note that the error bars from these measurements are much smaller than that achievable at RHIC. Figure 3.4-3 shows the projected  $R_{AA}$  for all the three separated states, taking into account the p+p reference from the average of the world data.

Collision system	Mini. lumi. for 10% uncertainty on $\Upsilon(3S)$	Mini. lumi. for 10% uncertainty on $\Upsilon(2S+3S)$
p+p 200 GeV	420 pb <sup>-1</sup>	150 pb <sup>-1</sup>
p+p 510 GeV	140 pb <sup>-1</sup>	50 pb <sup>-1</sup>
Au+Au 200 GeV	10 nb <sup>-1</sup>	3.8 nb <sup>-1</sup>

**Table 3.4-1:** Estimated luminosities for  $\Upsilon(2S, 3S)$  measurements.

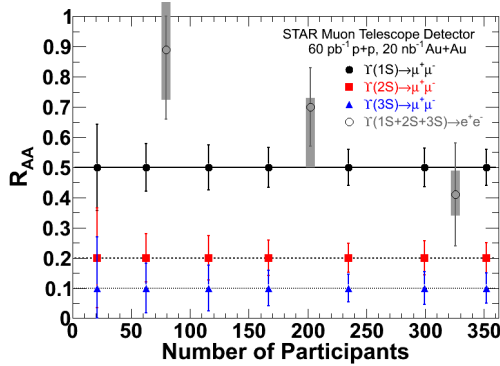


**Figure 3.4-3:** Projected errors on  $R_{AA}$  of Upsilon 1S+2S+3S measured by the STAR MTD from the 20 nb<sup>-1</sup> Au+Au and 60 nb<sup>-1</sup> p+p collisions (reference data).

The STAR MTD allows for the measurements of electron-muon correlations, where the electron and muon are both measured at mid-rapidity. The dominant source of these correlations at intermediate mass is from the decay of charm-anticharm pairs, since in thermal production of dilepton pairs electrons are paired with positrons, and muons with antimuons. In Run 12 p+p collisions at  $\sqrt{s}=200$  GeV STAR established that we can trigger on electron-muon pairs with one leg in the MTD and the other leg in the Barrel Electromagnetic Calorimeter (BEMC) at a transverse energy threshold of 1.9 GeV. This was a very clean trigger, running at prescale 1 with a very low rate ( $\sim 10^3$  of Hz) in the p+p collisions. The total sampled luminosity in run 12 was 23 pb<sup>-1</sup>. We expect that this trigger will be equally effective in Au+Au collisions allowing us to sample the entire set of luminosity delivered by RHIC with high efficiency. We can also sample a large fraction of the delivered luminosity with a central trigger, which enables the kinematic cuts to be relaxed to allow for lower energy electrons, identified via the ToF and TPC  $dE/dx$ .

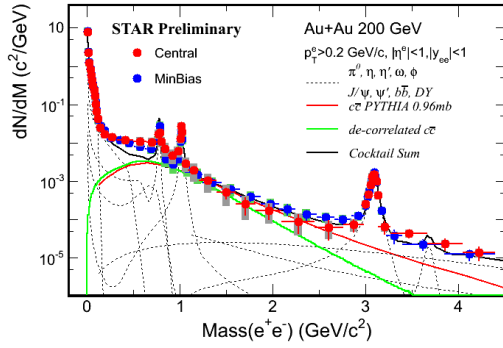


**Figure 3.4-4:** Central and minimum bias di-electron invariant mass distributions, from Run 10 Au+Au collisions. Central data has been scaled to match minimum bias at low invariant mass. Red line shows the cocktail contribution from fully correlated charm-anticharm pairs, assuming a cross section of 0.96 mb. Green line shows the contribution if charm is angularly decorrelated and momentum distributions softened to match non-photonic electron  $R_{AA}$

Figure 3.4-4 shows the existing minimum bias and central di-electron pair invariant mass distributions, where the central data has been scaled to match the minimum bias data at low invariant mass. According to the cocktail, the correlated charm contribution dominates the contribution in the intermediate mass range from 1 to 3  $\text{GeV}/c^2$ . In this figure, the correlated charm contribution is from PYTHIA, assuming no decorrelation in medium and rescaled to match a charm cross section of 0.96mb. Both of these assumptions introduce a large uncertainty, due to the possibility of charm energy loss and decorrelation in the medium, both of which would decrease the contribution in this mass range. There are hints of suppression in central as compared to minimum-bias data. This uncertainty prevents the extraction of any signal from QGP radiation, which in the absence of decorrelation is approximately an order of magnitude below the charm contribution. The only way to make progress is to directly measure the correlated charm contribution in heavy ion collisions: electron-muon correlations provide one method to do so.

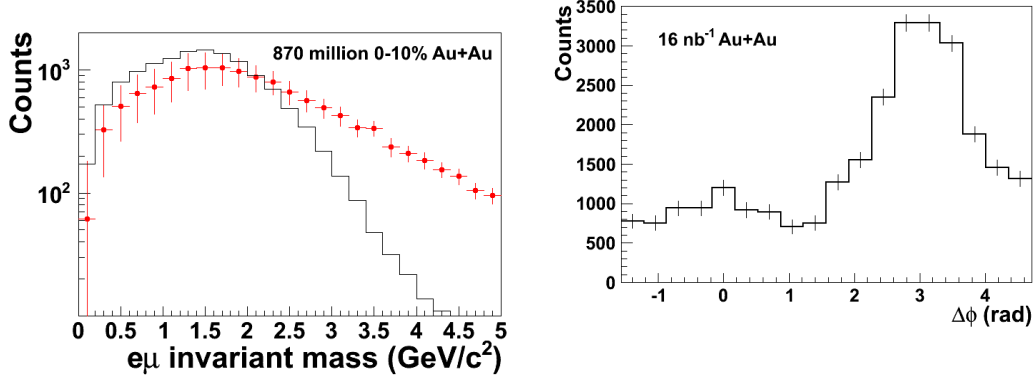


**Figure 3.4-5:** (Left) Projected electron-muon invariant mass distribution from 280M top 10% central Au+Au events and MTD coverage as in Run 13. Red points assume full correlation and momentum distributions from PYTHIA while the black histogram assumes full decorrelation and softening of the charm momentum distribution to match non-photonic electron  $R_{AA}$ . (Right) Projected electron-muon  $\Delta\phi$  distribution for electron  $p_T > 2 \text{ GeV}/c$ , for  $16 \text{ nb}^{-1} \text{ Au+Au}$  sampled by a trigger between an MTD hit on one leg and an electron in the Barrel Electromagnetic Calorimeter with  $E_T > 1.9 \text{ GeV}/c$ .

Figure 3.4-5 left plot shows the projected uncertainty in the electron-muon invariant mass distribution for 870M central 0-10% Au+Au events, assuming the PYTHIA fully correlated charm contribution. For comparison, the black histogram shows the maximal reduction in the distribution, assuming full angular decorrelation and suppression of the charm singles distribution following measured non-photonic electron  $R_{AA}$ . The proposed measurement can clearly distinguish this extreme scenario from the fully correlated PYTHIA scenario.

The downside of such triggered datasets is that they select specific regions of the invariant mass vs.  $p_T$  plane, and so need detailed comparisons with unbiased data and simulations under energy loss scenarios to interpret correctly. As a starting point, Figure 3.4-5 right plot shows the projected uncertainty on the  $\Delta\phi$  distribution between the electron and muon, with electron and muon  $p_T > 2$  GeV/c, with the expected strength of the correlation from PYTHIA, after sampling  $16 \text{ nb}^{-1}$  with the MTD-BEMC trigger. Angular decorrelation of charm-anticharm pairs would lead to a decrease of the height and/or broadening of the width of the away-side peak, which is clearly resolvable with this sample.

### 3.5. Gamma-Jet measurement

The  $\gamma_{\text{dir}}$ -jet coincidence measurements have long been proposed as a powerful tool, i.e. the golden probe of energy loss, to study parton energy loss in the medium [14]. The leading-order production processes of direct photons, quark-gluon Compton scattering ( $q+g \rightarrow q+\gamma$ ) and quark-antiquark annihilation ( $q+\bar{q} \rightarrow g+\gamma$ ), are free from the uncertainties accompanying fragmentation. The outgoing high- $p_T$   $\gamma$  balances the  $p_T$  of the partner parton separated by  $\pi$  in azimuth (“away-side”), modulo corrections due to parton intrinsic  $k_T$  [15] and “resummation” of soft-gluon effects [16,17]. The study of the spectra of the away-side jet particles associated with the high- $p_T$   $\gamma_{\text{dir}}$  can constrain the dependence of  $\Delta E$  on  $E$ . The mean-free path of the  $\gamma$  in the medium is large enough that its momentum is preserved, regardless of the position of the initial scattering vertex. The  $\gamma$  does not suffer from the geometric biases (non-uniform spatial sampling of hadron triggers due to energy loss in the medium) inherent in di-hadron azimuthal correlation measurements. A comparison between the spectra of the away-side particles associated with  $\gamma_{\text{dir}}$  vs. with  $\pi^0$  can constrain the dependence of  $\Delta E$  on  $L$  [18]. Also, comparisons between the associated particle yields for  $\gamma_{\text{dir}}$  triggers in- and out-of-plane and in different collision systems are additional probes of the path-length dependence of energy loss.

To leading order and in the asymptotic limit of very large jet energies, the mean multiplicities of quark and gluon jets are predicted to differ by the ratio of Casimir factors (9/4). In p+p, the dominant channel for  $\gamma_{\text{dir}}$  production is Compton scattering, in the covered phase space at mid-rapidity at RHIC energy. Thus quarks and gluons are present in different proportions on the away-side of the  $\gamma_{\text{dir}}$  and  $\pi^0$  triggers. A comparison between the associated particle yields associated with  $\gamma_{\text{dir}}$  vs. with  $\pi^0$  can constrain the  $\Delta E$  dependence of on parton type. It is difficult to disentangle this from the path-length dependence. Therefore, it is important to have as many handles on the

path-length dependence as possible (*i.e.* different collision systems as well measurements with respect to the reaction plane).

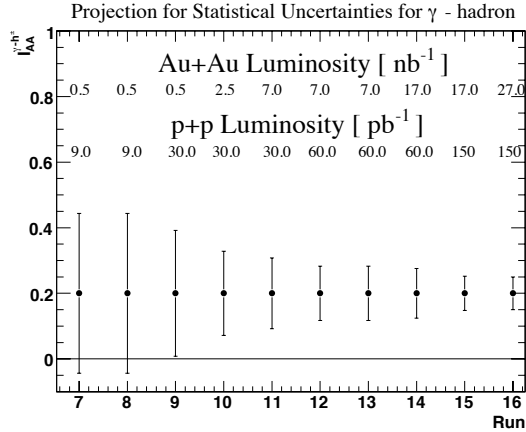


**Figure 3.5-1:** Projection for statistical uncertainties in  $\gamma$ -hadron suppression in a scenario of luminosity progression in different years. Projection is for  $E_T(\gamma) > 1$  GeV, associated particle  $p_T$  from 4-5 GeV/c.

Figure 3.5-1 shows the projection for statistical uncertainties in  $\gamma_{\text{dir}}$ -hadron suppression for  $E_T(\gamma) > 1$  GeV, and  $p_T = 4-5$  GeV/c for the associated particles.

In STAR experiment the required trigger for the  $\gamma_{\text{dir}}$  analysis is well established and has been commissioned and used for Run 7 and Run 10. The  $\gamma_{\text{dir}}$  trigger uses the same algorithm for the different collision systems. Currently we don't have any plan to change the level-2 algorithm of  $\gamma_{\text{dir}}$ ; however, we may increase the trigger energy threshold.

### 3.6. Beam energy scan program

**Introductions:** The study of QCD phase structures is one of the most important tasks for the RHIC facility. In the RHIC Beam Energy Scan Phase-I (BES-I) program, we have observed intriguing changes in several observables, such as the charged hadron nuclear modification factor  $R_{AA}$ , identified hadron anisotropic parameter  $v_2$ , and higher moments for net-protons, at a collision energy around  $\sqrt{s_{NN}} = 20$  GeV. These observed dramatic changes not only indicate the structure of the QCD phase diagram, but also further confirm the existence of the strongly-coupled QGP discovered at top collision energies at RHIC. However, the statistics collected for collisions at low energies are too small to allow making any firm conclusions regarding the nature of the media created in such collisions. In addition, the gap in baryon chemical potential between  $\sqrt{s_{NN}} = 19.6$  GeV and 11.5 GeV for Au+Au central collisions is more than 100 MeV, twice as large as between other neighboring energies. In order to take high statistics data at low energies, a second phase of the beam energy scan (BES-II) with electron-cooling has been proposed for RHIC by C-AD, and is expected to be realized in 2017. In the meantime, we propose to take  $\sqrt{s_{NN}} \sim 15$  GeV data, to fill the large gap between 19.6 GeV and 11.5 GeV noted above. The results will also help us devise an optimal strategy for BES-II. Based on the BES-I experience and C-AD predictions on luminosity, we propose to collect 150M events from Au+Au collisions at 15 GeV. This will require about three weeks of beam time at the given energy.

The motivation of the fixed-target mode running is to extend the range of baryon chemical potentials accessed during the BES-II program from the current maximum of about  $\mu_B \sim 420$  MeV (for the  $\sqrt{s_{NN}} = 7.7$  GeV collider system) up to  $\sim 775$  MeV (corresponding to the fixed-target center-of-mass energy of  $\sqrt{s_{NN}} \sim 2.5$  GeV) in the QCD phase diagram[19]. The goal of the fixed-target program is to find evidence of the first order phase transition through identification of the softest point. As illustrated in the left panel of Figure 3.6-1, at energies well below the phase boundary, it is expected that the systems created will respond to pressure following a pure hadron gas equation of state. As the energy is increased, systems are created that enter the mixed phase region [20-22]. The phase coexistence region is thermodynamically unstable and exhibits very low incompressibility (softening of the equation of state) [23]. Systems that have just enough energy to achieve the onset of deconfinement will spend the maximum time in the unstable region (maximum time  $\sim$  softest point). As the energy increases further, the maximum compression point of the phase trajectory, illustrated as a burst in the left panel of Figure 3.6-2, moves deeper inside the plasma region, and one expects the system to respond to pressure following a partonic equation of state. Evidence has been presented to suggest that the onset of deconfinement is achieved for symmetric collisions at  $\sqrt{s_{NN}} = 7.7$  GeV [24], therefore it is prudent that searches for the softest point include energies both above and below 7.7 GeV. The fixed-target program allows the region below this suggested onset energy to be explored. The physics observables to be studied are the directed flow of net-protons, which has to be a very promising signature for a softening of the EOS, the inclusive elliptic flow, which has shown an interesting inflection at the low end of the BES energy range, and the azimuthal HBT of pions.

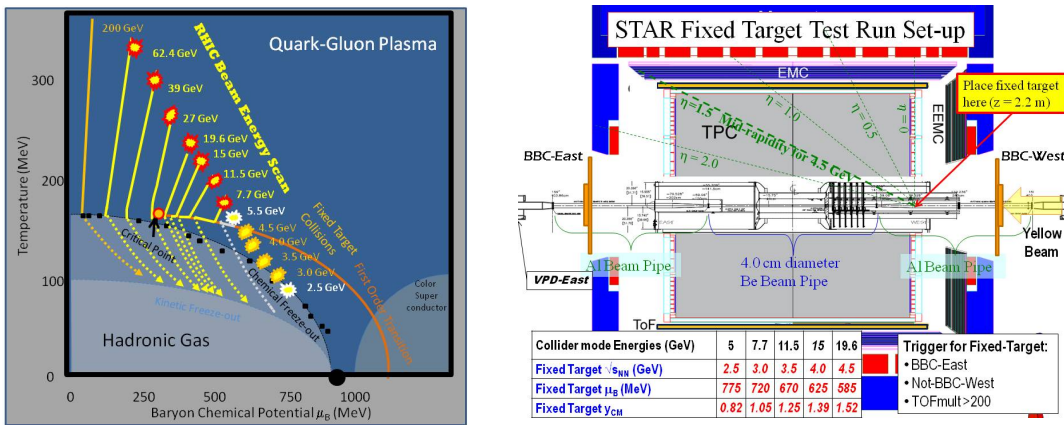


**Figure 3.6-1:** (Left) A cartoon of the phase diagram of nuclear matter showing possible trajectories for the expansion stage for reactions from BES collision systems. The red bursts represent the hottest and densest stage of the collision once thermodynamic equilibrium has been achieved. The yellow lines indicate the trajectory of the system during its expansion. The fixed-target points are shown with orange bursts. The 5.5 GeV collider system and corresponding 2.5 GeV point have not been demonstrated to provide a viable data sample; therefore they are shown in white. (Right) A schematic of the experimental set-up shows the location of the fixed-target and pseudo-rapidity lines to give a sense of the acceptance ranges.

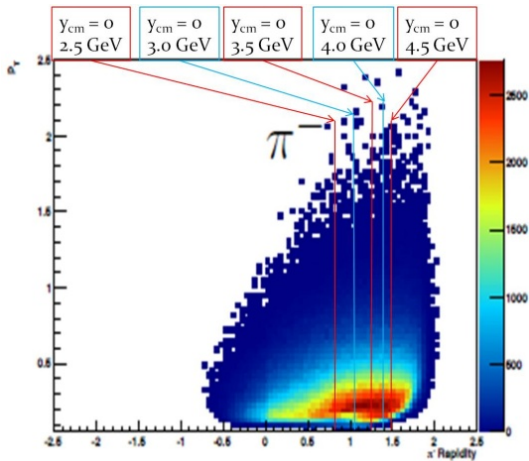


**Figure 3.6-2:** The acceptance of the STAR detector for negative pions. The data are from background interactions.

**Request for Run14:** The fixed-target capabilities of the STAR detector have been explored using interactions between nuclei in the beam halo and nuclei in the aluminum portion of the beam pipe. These data were taken as background events during the BES-I data taking in Runs 10 and 11. These exploratory studies have demonstrated that STAR will have acceptance at mid-rapidity for interactions with projectile energies at or below the nominal RHIC injection energy of 9.8 GeV. As illustrated in Figure 3.6-1 (right), the detector will have a window of acceptance that covers about 1.5 units in rapidity with full azimuthal coverage. The detector performs well for the basic functions of tracking, particle identification, and momentum resolution. These studies have demonstrated that adding a fixed-target program to STAR will extend the scientific reach of the BES-II program. The fixed-target program is well suited to run in conjunction with the BES-II because its ideal projectile energy range matches the energies proposed for BES-II.

Although the detector has been demonstrated to work well with fixed-target geometries for sub-injection energy projectiles, there are still two important questions that must be answered with test run time in Run14. First, we must determine how STAR can selectively trigger on interactions between projectile nuclei and the installed fixed-target. Secondly we must determine whether there are gold nuclei in the halo or if the beam must be intentionally steered in order to deliver gold nuclei onto the target.

In order to understand the background caused by the interactions on the beam pipe, we will need two 30-minute test runs early in the ion running of Run 14. These runs should each use only the yellow beam circulating at injection energy. We will take data for 30 minutes. We will then need one week to analyze the events and to determine the efficiency with which the trigger can select events originating within the target from the very high background coming from interactions with the beam pipe and other material. The second 30 minute run will be needed to refine the settings for the trigger.

In the past, we have studied interactions between beam halo and target nuclei, however, it has not been determined whether the halo is made up of projectile fragments from upstream nuclear interactions or elastically scattered gold nuclei. Therefore, at the end of the 200 GeV gold running period, we will need a full eight hour test run. During this

run, we will intentionally steer the beam. This operation does entail some risk and may require removal of the pixel detector of the HFT, which should be possible in two shifts [25]. In order to minimize risk, we will start with only a single bucket in the yellow beam at injection energy. The beam gradually will be lowered to bring the edge of the beam onto the target. Count rates will be monitored carefully with scalers to determine when the beam starts to graze the edge of the target (a test simulating this operation was performed by CAD on 01-May-2013). These data are needed to determine whether there were usable gold nuclei in the beam halo that was studied previously in Runs 10 and 11 and in the first test run of Run 14. If it is determined that there are usable gold ions in the halo, the fixed-target program can be run parasitically during BES-II. If it is determined that it is necessary to steer the beams to deliver gold ions onto the target, this will require a different running configuration (i.e. dedicated runs) for the fixed-target program. This test run will allow us to determine the beam time requirements should dedicated runs be needed.

Fixed-target data at  $\sqrt{s_{NN}} = 4.0$  GeV will be taken parasitically during this run. The results of the two test runs described in the previous paragraphs will determine if the data taken parasitically using the beam halo contain gold nuclei or heavy projectile fragments, in which case a separate test run in which the yellow beam is steered may be necessary. The data from this 4.0 GeV run will be the first significant Au+Au data set that STAR accumulates below the proposed onset of deconfinement at 7.7 GeV.

In order for this fixed-target program to go forward in Run 14, it will be necessary to complete the design, engineering, fabrication, and safety review for the internal target in a timely manner that allows installation of the target during the summer 2013 shutdown.

## References:

- [1] B. I. Abelev *et al.* [STAR Collaboration], Phys. Rev. Lett. 98, 192301 (2007); Erratum, Phys. Rev. Lett. 106, 159902(E) (2011).
- [2] Yu. L. Dokshitzer and D. E. Kharzeev, Phys. Lett. B 519, 199 (2001).
- [3] M. Djordjevic M. Gyulassy, R. Vogt and S. Wicks, Phys. Lett. B 632, 81 (2006); R. Sharma, I. Vitev and B.-W. Zhang, Phys. Rev. C 80, 054902 (2009); H. van Hees, V. Greco and R. Rapp, Phys. Rev. C 73, 034913 (2006).
- [4] Y.F. Zhang (for STAR Collaboration), QM 2011 proceedings; D. Tlusty (for STAR Collaboration), QM 2012 proceedings.
- [5] HFT proposal, [http://rnc.lbl.gov/~wieman/hft\\_final\\_submission\\_version.pdf](http://rnc.lbl.gov/~wieman/hft_final_submission_version.pdf).
- [6] W. A. Horowitz and M. Gyulassy, Phys. Lett. B 666, 320 (2008).
- [7] X. Dong *et al.*, Phys. Lett. B 597, 328 (2004).
- [8] G. Moore and D. Teaney, Phys. Rev. C 71, 064904 (2005); H. van Hees and R. Rapp, Phys. Rev. C 71, 034907 (2005).
- [9] X. Zhu, P. Zhuang, and N. Xu, Phys. Rev. Lett. 100, 152301 (2008).
- [10] P. Sorensen and X. Dong, Phys. Rev. C 74, 024902 (2006).
- [11] H. van Hees *et al.*, Eur. Phys. J. C 61, 799 (2009).
- [12] G. Agakishiev *et al.* [STAR Collaboration], Phys. Rev. Lett. 108, 072302 (2012).

- [13] L. Adamczyk *et al.* [STAR Collaboration], submitted to Phys. Rev. Lett., December, 2012. arXiv: 1212.3304.
- [14] X.-N.Wang, Z. Huang and I. Sarcevic, Phys. Rev. Lett. 77, 231 (1996).
- [15] L. Cormell and J. F. Owens, Phys. Rev. D 22, 1609 (1980) and references therein.
- [16] A. Kulesza, G. Stermann, and W. Vogelsang, Nucl. Phys. A 721, 591 (2003).
- [17] P. Aurenche *et al.*, Phys. Rev. D 73, 094007 (2006).
- [18] T. Renk and K. Eskola, Phys. Rev. C 75, 054910 (2007).
- [19] The translation between center-of-mass energy and chemical potential follows imperial relations detailed in J. Cleymans, H. Oeschler, K. Redlich, S. Wheaton, PR C73, 034905 (2006).
- [20] I. C. Arsene *et al.*, Phys. Rev. C **75**, 034902 (2007).
- [21] J. Randrup, Phys. Rev. C **82**, 034902 (2010).
- [22] J. Randrup, Phys. Rev. C **79**, 054911 (2009).
- [23] V. Koch, A. Majumder, J. Randrup, Phys. Rev. C **72**, 064903 (2005).
- [24] NA49 Collaboration, Phys. Rev. C **77**, 024903 (2008).
- [25] The [http://www4.rcf.bnl.gov/~videbaks/hft/cd1/HFT\\_CDR\\_V26.pdf](http://www4.rcf.bnl.gov/~videbaks/hft/cd1/HFT_CDR_V26.pdf).

## 4. Study of p+p and p+A Collisions

### 4.1. Introduction

The STAR spin physics program seeks to advance our understanding of the spin and flavor structure of the proton in terms of its constituent quarks and gluons, exploiting the unique capability of RHIC to provide access to polarized p+p collisions. Using longitudinally polarized beams, one can probe the helicity preferences of the gluons and (flavor-separated) antiquarks, to determine the contribution of each to the total spin of the proton. With spins transverse to their momentum direction, the p+p collisions exhibit kinematic and dynamical effects that are directly sensitive to quark transversity and partonic motion within the proton, e.g., orbital angular momentum. This program is complemented by studies of polarized p+p elastic scattering and central exclusive production, in which a far-forward proton is detected intact.

Since 2009 RHIC has just completed several very successful polarized p+p runs both at  $\sqrt{s} = 200$  GeV and  $\sqrt{s} = 510$  GeV. The STAR recorded luminosity and the average beam polarization as measured by the H-jet polarimeter are summarized in Table 4.1-1.

Year	$\sqrt{s}$ (GeV)	Recorded Luminosity for Transverse p+p	Recorded Luminosity for Longitudinal p+p	$\langle P \rangle$
2009	200		25 pb <sup>-1</sup>	55
	500		10 pb <sup>-1</sup>	39
2011	500	25 pb <sup>-1</sup>	12 pb <sup>-1</sup>	48
2012	200	22 pb <sup>-1</sup>		61/58
	510		82 pb <sup>-1</sup>	50/54
2013	510		220 pb <sup>-1</sup> (till 22 May)	54/55

**Table 4.1-1:** The STAR recorded luminosity and the average beam polarization as measured by the H-jet polarimeter.

In Run 13 STAR collected to date 2.7 times the Run 12 data set with longitudinal polarization at  $\sqrt{s} = 510$  GeV. The beam polarizations attained at 510 GeV has stately increased from Run 9 and reached up to 60%. More detail on both RHIC and STAR performance in Run 13, and a brief look at the quality of results that can be expected, are provided in section 4.3 below. To build on these successes we request 12 weeks of polarized p+p operation at  $\sqrt{s} = 200$  GeV in Run 15. Essentially the data would be taken with beams longitudinally and transversely polarized at STAR. If we conservatively estimate that the sampled luminosity and polarization would be similar to that demonstrated in Run 12 for Run 15, such we could achieve 90 pb<sup>-1</sup> in 12 weeks

running, this would allow us to collect an additional 50 pb<sup>-1</sup> and 40 pb<sup>-1</sup> of longitudinal and transversely polarized data, respectively. Such a data set would significantly advance the STAR spin physics effort; in particular, our analyses would focus on:

- The impact of the increased precision in measurements of the double-spin asymmetry  $A_{LL}$  in inclusive jet and coincident di-jet production is discussed in chapter 4.4
- The increased statistics in transverse polarized data together with the new equipment installed for run-15 will allow us to address the underlying  $A_N$  process and dynamics by measuring less inclusive observables, i.e. IFF, jets and direct photons. Details are discussed in chapter 4.5

## 4.2. Recent highlights from the spin program

Since the last RHIC PAC, ongoing analyses of polarized p+p data acquired in earlier runs have led to many new results, a few of which are highlighted here.

The inaugural run at  $\sqrt{s} = 500$  GeV in 2009 yielded a first measurement of the longitudinal single-spin asymmetry  $A_L$  in  $W^\pm$  production, followed by rapid publication of this essential milestone [1]. The rapid analysis of the high statistics 2012 data set (85 pb<sup>-1</sup> with 55.6%/57.7% polarization) with longitudinal polarization at  $\sqrt{s} = 510$  GeV yielded the first results for  $W^\pm$  providing impact on the light sea quark polarizations. The STAR preliminary results on  $A_L^{W^\pm}$  taken during 2012, shown in Figure 4.2-1, have been included in the DSSV++ pQCD-fit. Figure 4.2-2 shows the results for the  $\chi^2$  profile for the truncated integral for  $\Delta\bar{u}$  and  $\Delta\bar{d}$  in the range  $0.05 < x < 1$  at  $Q^2=10$  GeV<sup>2</sup>. A clear improvement on the determination of the polarization of the light sea quarks is observed. For  $\Delta\bar{u}$  a shift away from the current best mean value is observed, reflecting that the new STAR  $A_L^{W^-}$  data lie above the central curve based on DSSV+. Already, with only the preliminary 2012 STAR data, the new global analysis shows a preference for  $\Delta\bar{u} > \Delta\bar{d}$  in the range  $x > 0.05$ .

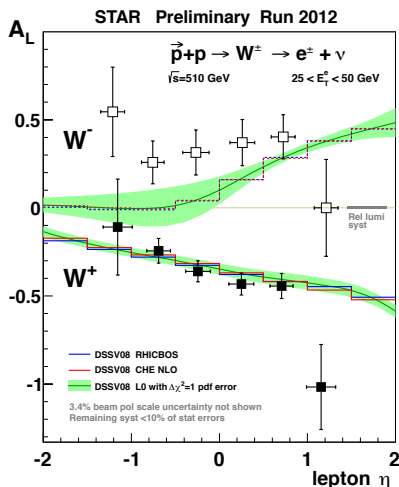


**Figure 4.2-1:**  $A_L$  for  $W^\pm$ , as a function of rapidity, as measured by STAR in 2012.

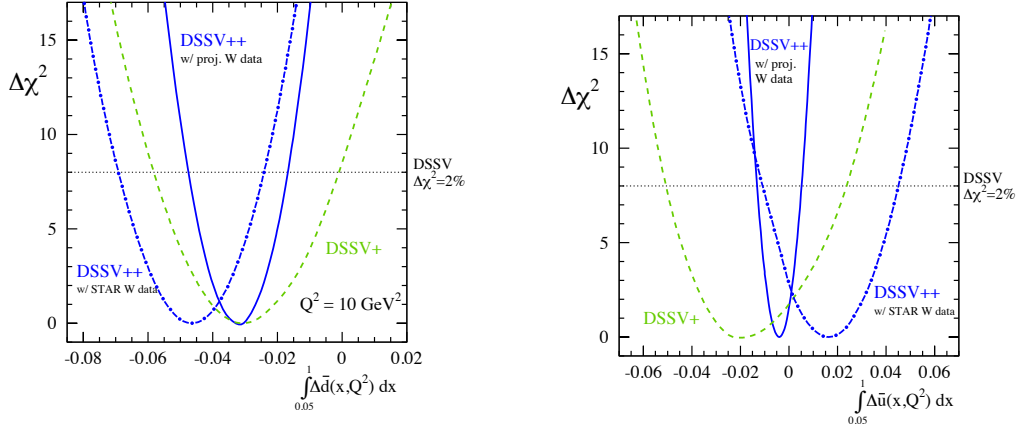


**Figure 4.2-2:**  $\chi^2$  profiles for  $\Delta\bar{u}$  (left) and  $\Delta\bar{d}$  (right) with (DSSV++) and without (DSSV, DSSV+). In the  $\chi^2$  profiles we also illustrate the impact of the preliminary 2012 STAR data from the left frame of Fig. 4 (blue dashed-dotted curves).

In 2009, with improved luminosity and polarization, as well as upgraded triggering and data acquisition systems at STAR, both experiments improved considerably the uncertainties in  $A_{LL}$  measurements at  $\sqrt{s}=200$  GeV. The impact of these data on global QCD fits based on the DSSV framework is illustrated in Figure 4.2-3 and Figure 4.2-4. The fit labeled DSSV+ supplements the RHIC data used in the original DSSV analysis with recent results from polarized deep-inelastic scattering (DIS) obtained by COMPASS [4], and the results denoted as DSSV++ include, in addition, the 2009 STAR data shown in Figure 4.2-2(left). The preliminary DSSV++ fit is fully consistent with the previous DSSV fit within the uncertainties and shows a preference for a sizable (relative to the total proton spin of  $1/2\hbar$ ) gluon contribution,  $\int_{0.03}^{0.2} \Delta g(x) dx = 0.1 \pm_{0.07}^{0.06}$  with significantly reduced uncertainties. Despite this very important achievement, uncertainties for  $\Delta g(x)$  remain significant in the presently unmeasured small  $x$  region and prevent a reliable determination of the full integral, see Figure 4.2-4. By comparing  $\Delta g(x)$  integrated in the  $x$ -range presently covered by RHIC with the integral for the sum of the polarized quark densities  $\int_{0.001}^1 \Delta\Sigma(x) dx = 0.366 \pm_{0.062}^{0.042}$ , as determined from DIS data [3], it can be seen that despite the different  $x$ -ranges gluons can make a very significant contribution to the spin of the proton.

A natural next step in the investigation of nucleon structure is an expansion of our current picture of the nucleon by imaging the proton in both momentum and impact parameter space. At the same time we need to further our understanding of color interactions and how they manifest in different processes. In the new theoretical framework of transverse momentum dependent parton distributions (TMDs) we can obtain an image in the transverse as well as longitudinal momentum space (2+1 dimensions). This has attracted renewed interest, both experimentally and theoretically in transverse single spin asymmetries (SSA) in hadronic processes at high energies, which have a more than 30 years history. First measurements at RHIC have extended the observations from the fixed-target energy range to the collider regime. Future PHENIX and STAR measurements at RHIC with transversely polarized beams will

provide unique opportunities to study the transverse spin asymmetries in Drell-Yan lepton pair, direct photon, and W boson productions, and other complementary processes. Also evolution and universality properties of these functions can be studied. Polarized nucleon-nucleus collisions may provide further information about the origin of SSA in the forward direction and the saturation phenomena in large nuclei at small  $x$ .

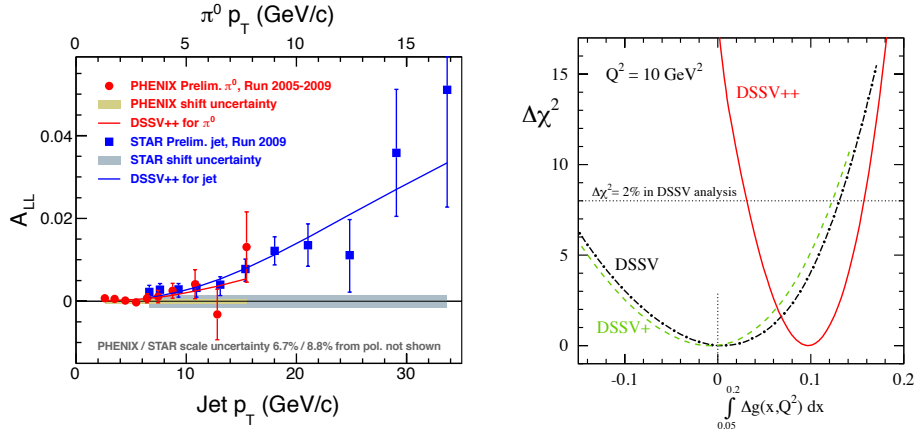


**Figure 4.2-3:** Preliminary 2009 jet data compared to the DSSV++ fit (**left**) and the  $\chi^2$  profile for the integrated gluon contribution in the  $x$  region currently probed at RHIC for  $\sqrt{s} = 200 \text{ GeV}$  (**right**). The different  $p_T$ -scales for  $\pi^0$ s and jets reflect that an individual  $\pi^0$  carries only a fraction of the scattered parton momentum.

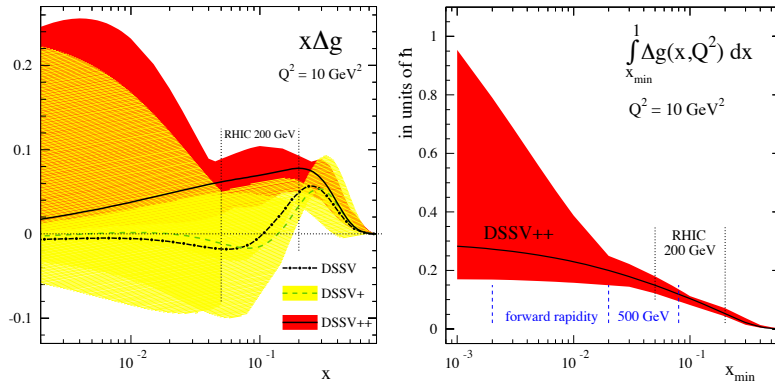


**Figure 4.2-4:** Uncertainties in  $\Delta g(x)$  with (red band) and without (yellow band) RHIC 2009 data (**left**) and in the integral computed in the range from  $x_{min}$  to 1 (**right**) at a scale of  $10 \text{ GeV}^2$ . The flexible functional form for  $\Delta g(x)$  used in the DSSV analysis [3] was utilized in all fits.

Single spin asymmetries in inclusive hadron production in proton-proton collisions have been measured at RHIC for the highest center-of-mass energies to date,  $\sqrt{s} = 500 \text{ GeV}$ , summarizes the measured asymmetries from different experiments as functions of Feynman- $x$  ( $x_F \sim x_1 - x_2$ ) and transverse momentum. Surprisingly large asymmetries are seen that are nearly independent of  $\sqrt{s}$  over a very broad range. To understand the observed significant SSAs one has to go beyond the conventional collinear parton picture in the hard processes. Two theoretical formalisms have been proposed to

generate sizable SSAs in the QCD framework: transverse momentum dependent parton distributions and fragmentation functions, which provide the full transverse momentum information. At RHIC the  $p_T$ -scale is sufficiently large to make the collinear quark-gluon-quark correlation formalism, which provides the average transverse information, also an appropriate approach to calculate the spin asymmetries.

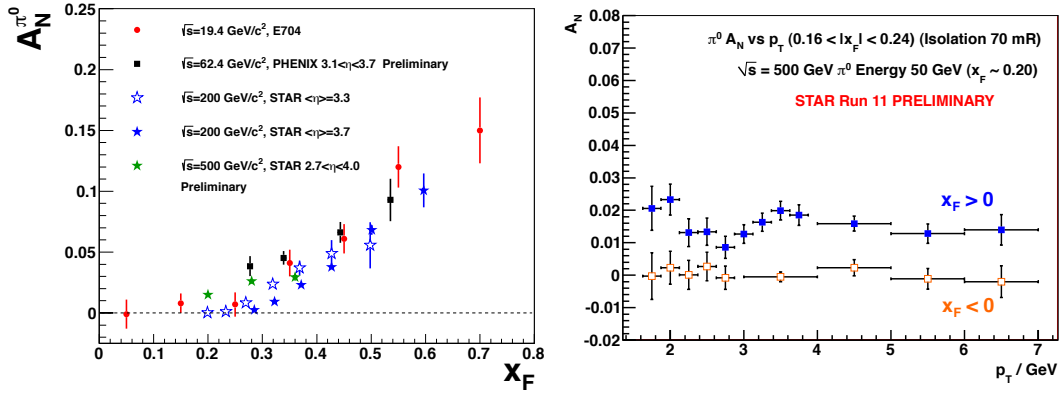


**Figure 4.2-5:** Transverse single spin asymmetry measurements for neutral pions at different center-of-mass energies as function of Feynman- $x$  (left) and  $p_T$ -dependence at  $\sqrt{s} = 500$  GeV (right).

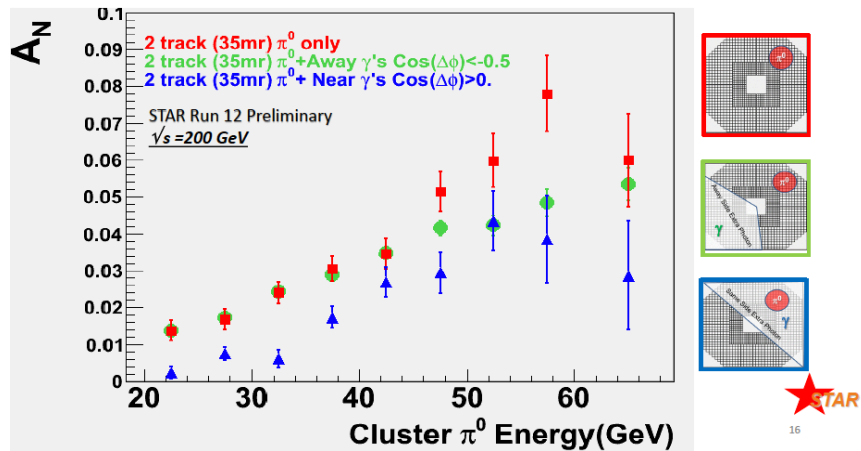


**Figure 4.2-6:**  $A_N$  for  $\pi^0$  as a function of the  $\pi^0$  Energy averaged over the pseudo-rapidity of the  $\pi^0$  and its  $p_T$  with a 35 mrad cone around the  $\pi^0$ . The blue and green points require additional activity outside the  $\pi^0$  isolation cone, the requirements are indicated in the schematics on the right side. These results make it even more important to extract observables, which are less inclusive.

STAR has made several important contributions to this program, primarily through study of forward neutral pion production in p+p collisions (see, for example, ref. [5] and Figure 4.2-5). This effort has recently been extended to include the first measurements at  $\sqrt{s} = 200$  GeV of the transverse spin asymmetry  $A_N$  for the  $\eta$  meson, a member of the pseudo-scalar octet that is also isospin  $I_3$ , like the  $\pi^0$ . The Run 11 transverse polarized data taken at  $\sqrt{s} = 500$  GeV allow to reveal one more surprising

feature the flat dependence of  $A_N$  for  $\pi^0$  as function of  $p_T$ , see Figure 4.2-5 (right). The high statistics transverse polarized data taken at  $\sqrt{s} = 200$  GeV in Run 12 confirm this behavior. But more importantly the Run 12 data allow studying in more detail the dependence of the  $\pi^0$   $A_N$  on the event kinematics.

As one can see in Figure 4.2-6, the asymmetry grows as more isolated the  $\pi^0$  is, which is in contradiction to what is expected for the Sivers-effect, which should be biggest in jet-like events.

Sivers	Transversity $h(x)$ x Collins FF
$A_N$ as function of rapidity and $E_T$ for inclusive jets $A_N$ as function of rapidity and $E_\gamma$ for direct photons $A_N$ as function of rapidity and $p_T$ for charmed mesons	Di-hadron correlations within a jet <ul style="list-style-type: none"> <li><math>A_N</math> as function <math>p_T</math> and the invariant mass of the hadron pair (IFF)  <math display="block">A_{UT}^{\sin\Phi} = A_{UT} \sin(\Phi_R - \Phi_S) = \frac{\sigma^\uparrow - \sigma^\downarrow}{\sigma^\uparrow + \sigma^\downarrow} \sin(\Phi_R - \Phi_S).</math></li> <li><math>A_{UT}</math> as function of the azimuthal dependence of the correlated hadron pair on the spin of the parent quark</li> </ul>

**Table 4.2-1:** Observables to separate the contributions from initial and final states to the transverse single spin asymmetries.

Table 4.2-1 identifies observables, which will help to separate the contributions from initial and final states, and will give insight to the transverse spin structure of hadrons. With its broad acceptance for charged particles in the TPC, STAR is well positioned to carry out the study of di-hadron correlations within a jet, *i.e.*, at relatively small opening angle, where one works with the transverse momentum  $p_T$  and the invariant mass of the pair, rather than with individual particle  $p_T$ . These Correlations can be described in terms of the product of the transversity  $h(x)$  and the so-called Interference Fragmentation Function, IFF, which is a chiral-odd quantity. Extracting the IFF in polarized  $p+p$  collisions at high energy is of particular interest as it will constrain  $h(x)$  at higher values of  $x$  than competing measurements in semi-inclusive DIS. Recent first results are shown in Figure 4.2-7.

The second observable is of leading charged pions inside a reconstructed jet. In this case one is looking for correlations between the azimuthal distribution of the pion inside the jet and the spin orientation of the parent proton. Similarly to the IFF case, these correlations are sensitive to the product of transversity  $h(x)$  and the Collins Fragmentation Function  $\Delta D(z)$ , also a chiral odd quantity. Measurements in semi-inclusive deep inelastic and electron-positron scattering have shown  $\Delta D(z)$  to be sizable and increasing with increasing pion momentum fraction  $z$ .

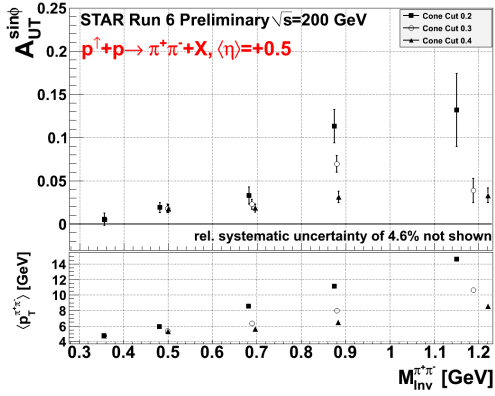


**Figure 4.2-7:** (top) Preliminary measurements of the transverse single-spin asymmetry  $A_{UT}$ , as defined in the text, as a function of the invariant mass of the unlike-sign di-pion. The choice of cone cut radius is strongly correlated with the average transverse momentum of the pair, as can be seen in the kinematic plot (bottom).

Figure 4.2-8 shows a recent measurement of this Collins asymmetry  $A_N$  made using mid-rapidity jets reconstructed at STAR. It was calculated by forming the ratio of the sum of the  $\sin(\phi_h - \phi_s)$  weighted events and the sum of the polarization  $P$  weighted events. Systematic errors were conservatively estimated to be  $\pm 0.023$  for the  $\pi^+$  and  $\pi^-$  results independently.

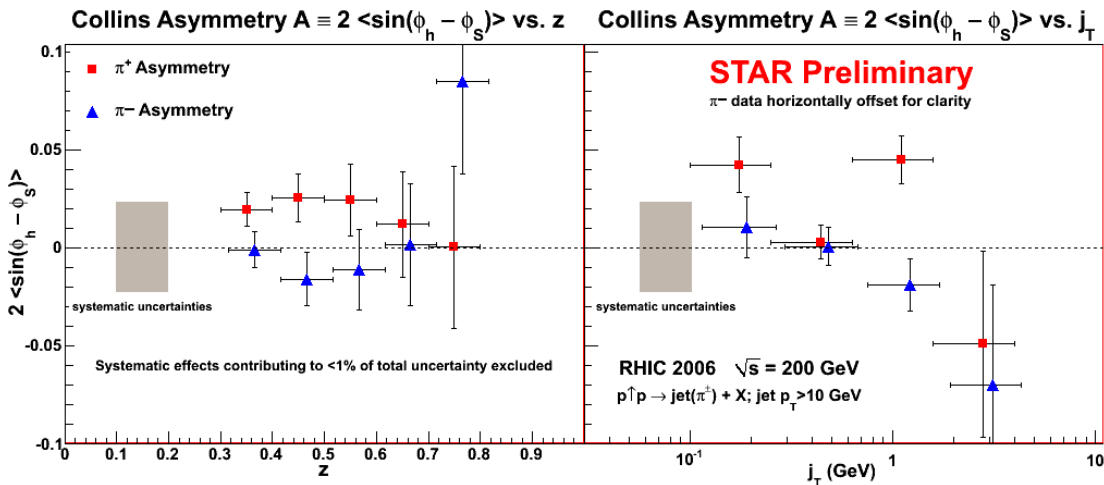


**Figure 4.2-8:** Preliminary results of the Collins moment for leading  $\pi^+$  (red) and  $\pi^-$  (blue) particles within mid-rapidity jets reconstructed by the STAR detector. Statistical errors are shown on data points and the grey shaded band indicates the systematic error bar for  $\pi^+$  and  $\pi^-$  separately.

Both the IFF and Collins analysis were exploratory measurements made using Run 6 transverse data. Indications of non-zero asymmetries motivated the extended 200 GeV running during Run 12 and for Run 15. Exceptional accelerator performance and high sampling rates at STAR during the 2012 run resulted in a sampled FOM of  $\sim 7.74 \text{ pb}^{-1}$  in 5 weeks, compared to the  $\sim 2.2 \text{ pb}^{-1}$  of transverse data taken in 2006 used in the STAR analysis, which indicate non-zero asymmetries. Data collected in Run 12 will allow these asymmetries to be measured with higher precision and increased kinematic coverage; see Figure 4.2-9 and Figure 4.2-10 for quantitative projections. These data will also be used to tighten the constraints on the mid-rapidity inclusive jet  $A_N$ , which will be dominantly sensitive to the gluon-Sivers contribution. At forward rapidities, the

2012 data will permit first steps to a measurement of the inclusive photon  $A_N$ , in the forward meson detector (FMS) at STAR.

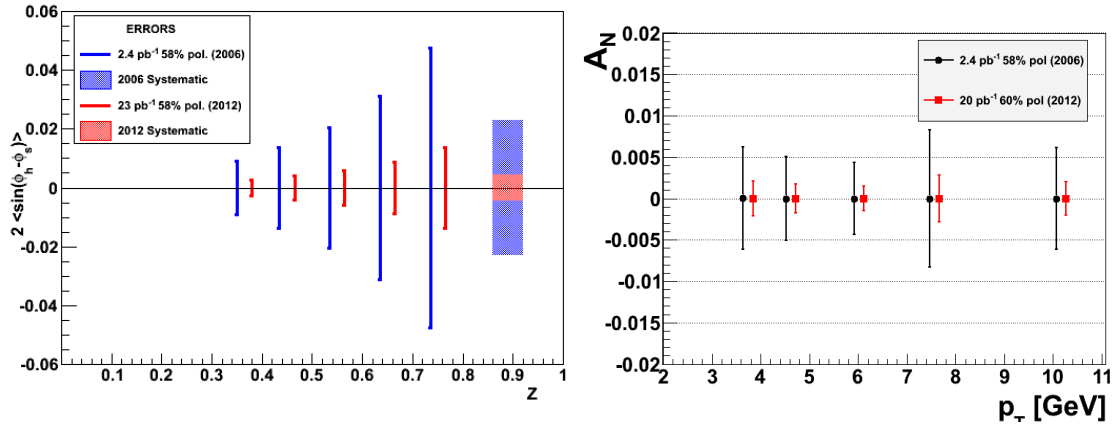


**Figure 4.2-9:** Run 6 errors compared to Run 12 ( $\sqrt{s} = 200$  GeV) projections for the ‘‘Collins-jet asymmetry’’ (left) and for the mid-rapidity Interference Fragmentation Function (right).

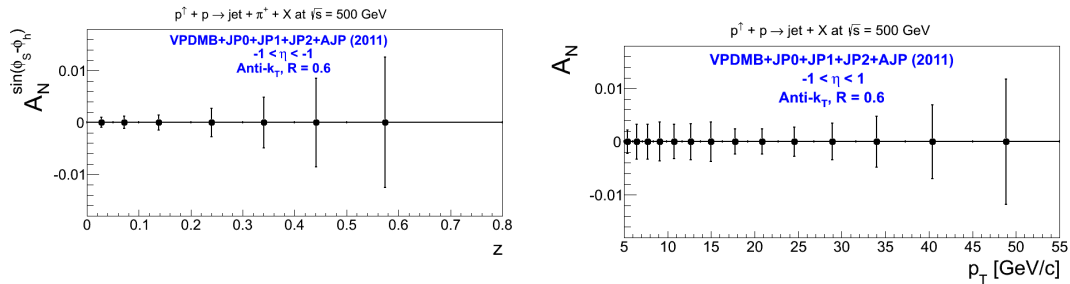


**Figure 4.2-10:** Uncertainties for the Collins (left) and Sivers (right) asymmetries as achieved from the Run-11  $\sqrt{s} = 500$  GeV data.

### 4.3. Run 15 request

STAR assumes for 2015 a run with 22 cryo-weeks, which are split in 12 weeks polarized p+A collisions and 5 weeks of transversely polarized p+p collisions. To allow for new physics observables, discussed in section 4.1 and 4.2, in polarized p+p and p+A collisions several smaller detector upgrades need to be realized.

1. the Roman pot system of pp2pp is moved to a new location in the DX-D0 region
2. a pre-shower detector is installed in front of the STAR FMS.

**Roman Pot Upgrade:** To address on one hand the recommendation by the PAC in their 2011 report to find a solution to run the pp2pp program to parasitic or concurrent running with the rest of the RHIC program, and to enable measurements like diffraction in p+p and p+A as well as exclusive  $J/\Psi$  production in ultra-peripheral p+p and p+A collisions, the Roman Pots are required to be relocated to the DX-D0 region. To stage

the costs for the full implementation of these upgrade an intermediate phase-II\* will be realized.

### 1. Summary of physics gain from Phase-II\* to Phase-II

Roman Pot in STAR Phase-I, Phase-II\* (aka Phase-IIa) and Phase-II:

- **Current configuration (Phase-I)** two horizontal (at 55.5m) and two vertical (at 58.5m) Roman Pots (RPs) each in outgoing Yellow and Blue beam (Detector:  $75 \times 45 \text{mm}^2$ )
- **Phase-II\*:** reconfiguration of Phase-I detectors. Two vertical RP each at  $\sim 15.2\text{m}$  and at  $\sim 17.3\text{m}$  (Detector: Phase-I detector)
- **Phase-II:** two vertical +one horizontal (at  $\sim 15.2\text{m}$ ) and two vertical and one horizontal (at  $\sim 17.3\text{m}$ ) RPs each (new Si-Detector:  $100 \times 70 \text{mm}^2$ )

A schematic layout of Phase-II\* is shown in Figure 4.3-1. A comparison between the x and y coverage as well as in the momentum transfer  $t$  to the proton for the RP in the Phase-II and Phase-II\* configuration is shown in Figure 4.3-2 and 4.3-3.

Phase-II\* has comparable  $t$  acceptance till  $0.8 \text{ GeV}^2$  as Phase-II, for physics studies at high  $t$  the full Phase-II needs to be realized. The design and location of Phase-II\* identified in collaboration with the CAD experts, allows the full implementation of Phase-II at a latter time. To have Phase-II\* realized for run-15 the design of the vacuum pipe needs to be finalized this summer, such that parts can be order and fabricated in time that the installation of the new vacuum chamber and the Roman Pots can be realized in the shutdown summer 2014.

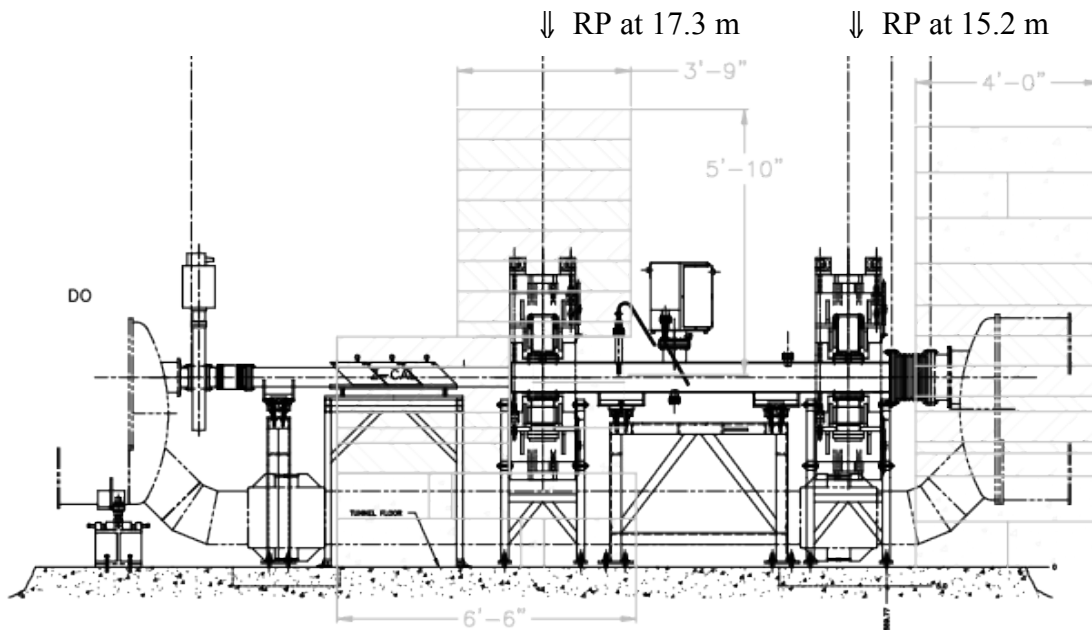


**Figure 4.3-1:** Proposed location and layout of Phase-II\* Roman Pots.

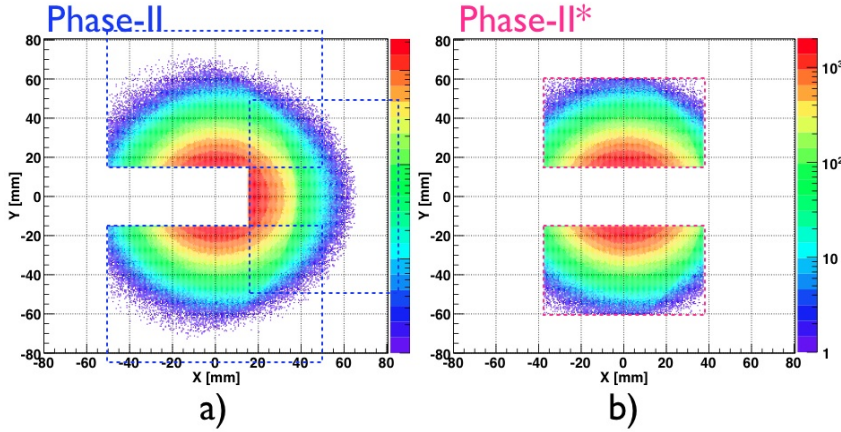


**Figure 4.3-2:** Distributions of protons at the upstream RPs for Phase-II a) and Phase-II\* b) configurations. The detector coverage is shown with dotted boxes.

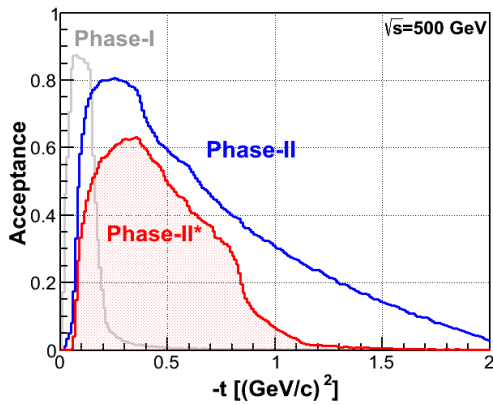


**Figure 4.3-3:** Acceptance protons from double Pomeron exchange processes in p+p at  $\sqrt{s} = 500$  GeV as function of  $t$  for Phase-II (blue) and Phase-II\* (red) configuration. The acceptance for Phase-I setup is also shown (grey).

**Pre-shower detector in front of the FMS:** To have cleaner electron identification for example for electrons from  $J/\Psi$ -decays, in the FMS the plan is to install a pre-shower detector in front of the FMS. The design follows closely a proposal of a pre-shower detector for the  $A_{NDY}$  experiment (see Figure 4.3-4).

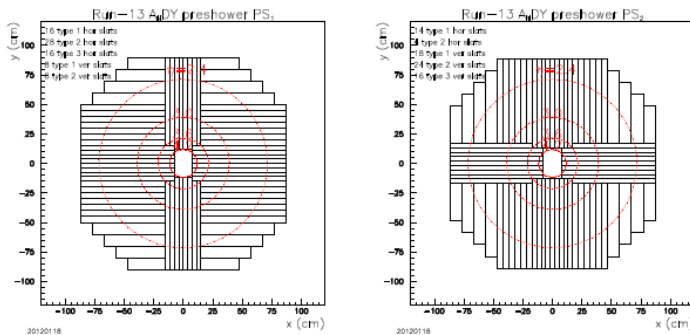


**Figure 4.3-4:** Proposed arrangement of pre-shower planes 1 (PS1, left) and 2 (PS2, right). Each plane consists of 76 total detectors each having a 0.5 cm thickness of BC-408 (primary component anthracene). There are three different slat widths used to tile the full acceptance of ECal: 3.75 cm; 5.0 cm and 10.0 cm. The PS1 and PS2 planes are located at smaller  $z$  values than a lead converter plate. Two planes are required for hermiticity. Parallel strips in each plane are staggered by half a strip width to ensure

that cracks between adjacent strips are not holes in the combined action of the two planes. A third plane of the same layout as PS1 is located at larger  $z$  than a  $\sim 1$  cm thick converter plate. The hermiticity requirement is not as severe for the PS3 plane since the converter most probably has initiated showers for electrons and positrons.

The pre-shower refers to a 3-plane system comprising two arrays of scintillator detectors (hereafter referred to as PS1, $i$  and PS2, $i$  where  $i$  refers to the segment number of the plane) that view the interactions with minimal intervening material, a planar Pb converter of known thickness and uniformity, and a final array of scintillator detectors (PS3, $i$ ) following the converter. The two planes before the converter are designed as hermetic as possible. The design assumes that a valid hit in either or both of the first two planes of the pre-shower will suffice for knowing that a charged particle created the hit. An electron or positron will most likely have a single minimum ionizing particle (MIP) response in PS1, $i$  (PS2, $i$ ) ( $\sim 95\%$ ), a PS3, $i$  response as given by multiple MIPs ( $\sim 98\%$ ), an energetic cluster in the FMS. A photon will most likely have little to no PS1, $i$  (PS2, $i$ ) response ( $\sim 98\%$ ) and a PS3, $i$  response as given by multiple MIPs ( $\sim 98\%$ ), and energetic cluster in the FMS. A charged hadron will most likely have a PS1, $i$  (PS2, $i$ ) and PS3, $i$  response as given by a MIP ( $\sim 99.8\%$ ), a MIP-like response in the FMS ( $\geq 33\%$ ). A neutral hadron will most likely have little to no PS1, $i$  (PS2, $i$ ) and PS3, $i$  response ( $\sim 99\%$ ), a small response in the FMS. A  $> 50$  photoelectrons response for a minimum-ionizing particle (MIP) passing through the detector is required. The uniformity requirement rules out configurations where photomultiplier tubes are used within the pre-shower acceptance to, for example, collect light from segments at large pseudorapidity. The pre-shower, especially the plane(s) before the converter, must be highly efficient to ensure robust  $\gamma$ /electron/hadron discrimination. Inefficiencies are mostly related to gaps between adjacent detectors. Our design first minimizes gaps by the construction methodology and secondly involves two scintillator planes before the converter to allow staggering of gaps. The PS1 and PS2 planes of the pre-shower will be followed by a sealed lead converter plate of thickness 1 cm (approximately 2 radiation length). Sealing of the lead will be accomplished by encasing it in adhesive-backed carbon fiber sheets. This encasing will then provide a robust means of mounting the converter in the pre-shower enclosure. A third plane of scintillator will follow the sealed lead converter plates. The object of this plane is to detect particles from showers initiated in the lead. Finite shower sizes make this plane less affected by cracks compared to scintillator before the lead. A glued construction will minimize cracks in any case. The geometry of PS1 will be chosen for PS3. Eight 32-channel QT boards, leaving 28 spare channels, will read out the total of 228 strips from the three planes. XP-2972 photomultiplier tubes at their ends distant from the beam could read out the detectors. A Cockcroft-Walton base powers each XP-2972.

First single particle GEANT simulations of the first 2 layers of the pre-shower detector response for 30 GeV electrons and photons show requiring  $0.5\text{MeV} < dE < 1.5\text{MeV}$  that 86% of electrons will be retained, while 98% photons will be rejected. For the 3<sup>rd</sup> pre-shower plane placed after 1cm Pb converter, responses for 30 GeV electrons, charged pion and photons are simulated, requiring an energy deposit above 5MeV 98% of the electrons will be retained, while 85% of pions and 39% of photons are rejected.

#### 4.4. Physics with 200 GeV longitudinally polarised p+p collisions

STAR aims to significantly improve its gluon polarization measurements at  $\sqrt{s} = 200$  GeV concurrent with the accumulation of proton-proton reference data for the HFT and MTD physics programs. The goal is to sample an additional  $50 \text{ pb}^{-1}$  with 60% longitudinal polarization in Run 15, making optimal use of the anticipated RHIC luminosity improvement afforded by the electron lenses.

Preliminary results, obtained in Run 9, on the double-spin asymmetry  $A_{LL}$  in inclusive jet production at  $\sqrt{s} = 200$  GeV from  $20 \text{ pb}^{-1}$  sampled with 58% average beam polarization are shown in Figure 4.2-3. The data with transverse momenta larger than  $\sim 12$  GeV/c are statistics and hence luminosity limited. The DSSV extraction [7] is shown as well, together with the 3-4 times less precise data from Run 6. The latter data are one of the inputs to the DSSV fit and provide unique sensitivity to the polarized gluon distribution for  $0.05 < x < 0.2$ . Even though the Run 9 data have, to date, not been included in a full update of the DSSV analysis, their high qualitative impact is easily assessed and a preliminary evaluation [13] has revealed for the first time the existence of a positive contribution from gluon spin to the proton spin at the level of 0.1 in the kinematic range accessed at RHIC.

Further improvement in the uncertainties is thus of particular interest. A reduction by a factor of nearly 2 is achievable at high  $p_T > \sim 12$  GeV/c while a smaller improvement by about  $\sqrt{2}$  is still achievable at smaller  $p_T$ . Doing so would provide significant further constraints on the polarized gluon distribution, especially for large momentum fractions  $x$ , and constitutes the main spin physics objective for Run 15 longitudinal running. The anticipated improvement and their complementarities with  $\sqrt{s} = 510$  GeV data are shown in Figure 4.4-1.

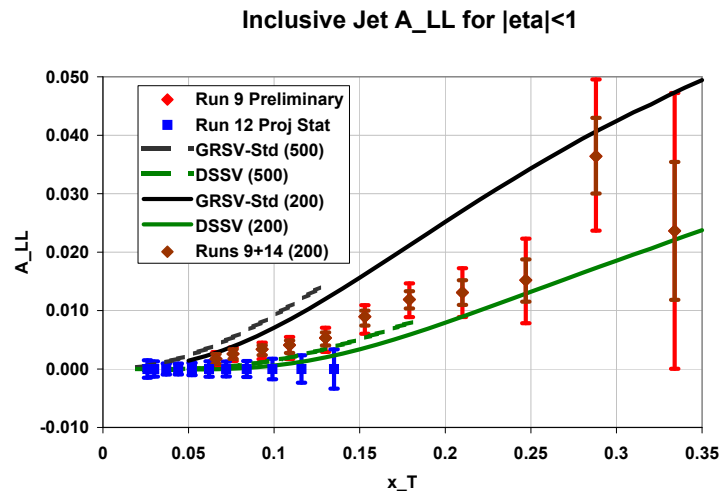


**Figure 4.4-1:** The expected precision for  $A_{LL}$  vs.  $p_T$  for inclusive jets at  $\sqrt{s} = 200$  GeV p+p collisions after the proposed Run 15 data are combined with the existing Run 9 measurements (brown diamonds). Also shown are the current Run 9 results (red diamonds) and the expected precision at  $\sqrt{s} = 510$  GeV from Run 12 (blue squares), together with model predictions for both energies from GRSV-Std and DSSV 2008.

A new data set of  $50 \text{ pb}^{-1}$  with 60% longitudinal polarization will also lead to significant improvement over the preliminary STAR measurements of di-jet  $A_{LL}$  at  $\sqrt{s} = 200 \text{ GeV}$ . Figure 4.4-2 shows the improvement of the  $\chi^2$  profile for the integrated gluon contribution in the  $x$  region currently probed at RHIC for  $\sqrt{s} = 200 \text{ GeV}$  including different data sets. The current uncertainties for  $\int_{0.03}^{0.2} \Delta g(x) dx = 0.1 \pm_{0.07}^{0.06}$  will be reduced by a factor of 2.

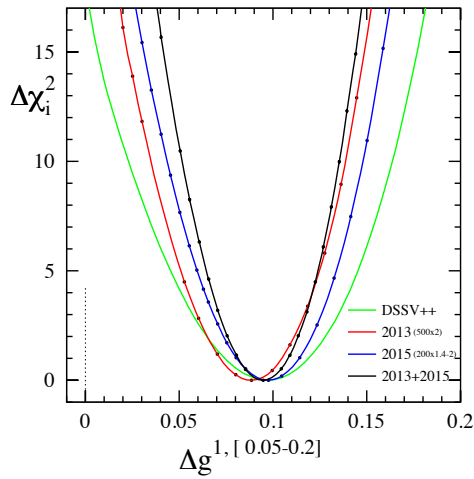


**Figure 4.4-2:** The improvement of the  $\chi^2$  profile for the integrated gluon contribution in the  $x$  region currently probed at RHIC for  $\sqrt{s} = 200 \text{ GeV}$ . The different curves represent including different data sets, red including the  $\sqrt{s} = 510 \text{ GeV}$  data from run 12 and 13 (red), blue including the expected data from run-15 (blue) and black represent a fit to all data at once.

STAR can extend the physics reach of its gluon polarization measurement by tapping the low- $x$  region accessible with both inclusive  $\pi^0$  and direct photon  $A_{LL}$  in the Forward Meson Spectrometer (FMS) at  $2.7 < \eta < 4.0$ . This important measurement will have a direct impact into any polarized NLO pQCD global analysis such as DSSV by supplying data in a previously unexplored kinematic zone.

#### 4.5. Physics with 200 GeV transversely polarised p+p collisions

Following the motivation for transverse polarized physics described in section 4.2 the transverse polarized p+p run with an integrated sampled luminosity of  $40 \text{ pb}^{-1}$  will allow to answer several open questions. Where does the  $p_T$ -dependence of  $A_N$  for  $\pi^0$  turn over from flat and follows the pQCD expected  $1/p_T$  behavior.

What are the underlying sub-processes being responsible for the forward  $A_N$ . Having a first measurement of the direct photons  $A_N$  with the FMS will be extremely crucial to understand the contribution of the Sivers-mechanism to the forward  $A_N$ . For the measurement of the direct photons it will be important to have the pre-shower described above installed in front of the FMS. Direct photons are rare process. Therefore it is important to suppress background from leptons, hadrons and  $\pi^0$  as much as possible. As shown by the first simulations the first 2 layers provide a lepton suppression of 98% by keeping 98% of photons, together with the third layer, which provides also 98% rejection of leptons and 85% rejection of hadrons, backgrounds can be suppressed

enough allow a measurement of  $A_N$  of direct photons. Figure 4.5-1 shows on the left side theoretical prediction from Ref. [16] using different assumptions or the Siverson function. On the right hand side the projected uncertainty for the prompt photon (= direct – fragmentation photon)  $A_N$ . The uncertainty in the fragmentation photon  $A_N$  was set to 5% The  $40 \text{ pb}^{-1}$  will allow for a measurement, which will be easily able to distinguish between the different model assumptions.

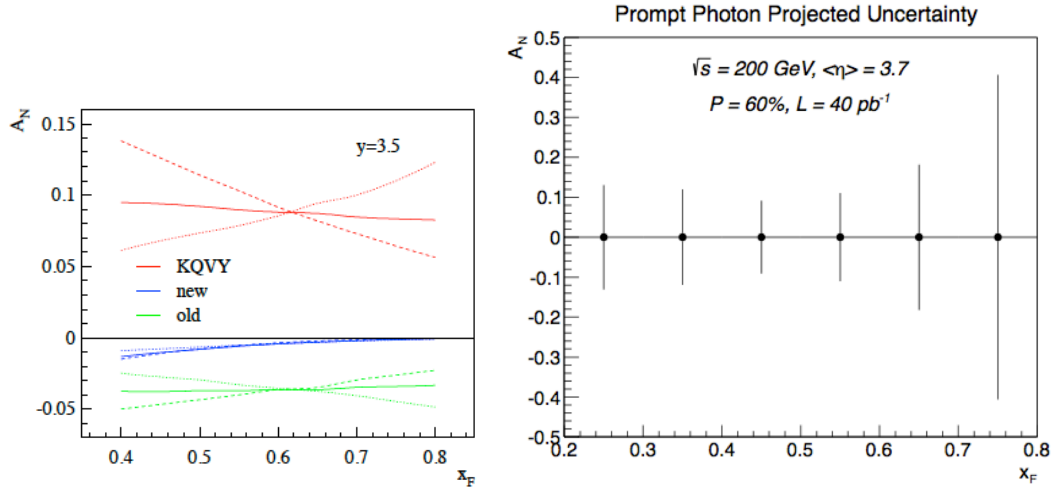


**Figure 4.5-1:** (Left plot) Single transverse spin asymmetry for prompt photon production,  $p^l+p \rightarrow g + X$ , plotted as a function of Feynman  $x_F$  at rapidity  $y = 3.5$  and  $\sqrt{s} = 200 \text{ GeV}$ . For each colored curve, the dashed curve is the direct asymmetry  $A_N^{\text{dir}}$ , the dotted curve is the fragmentation asymmetry  $A_N^{\text{frag}}$ , and the solid curve is the overall spin asymmetry. The different colors represent different assumptions about the magnitude of the Siverson asymmetry. (Right plot) The projected uncertainty for the prompt photon (=direct–fragmentation photon)  $A_N$ . The uncertainty in the fragmentation photon  $A_N$  was set to 5%.

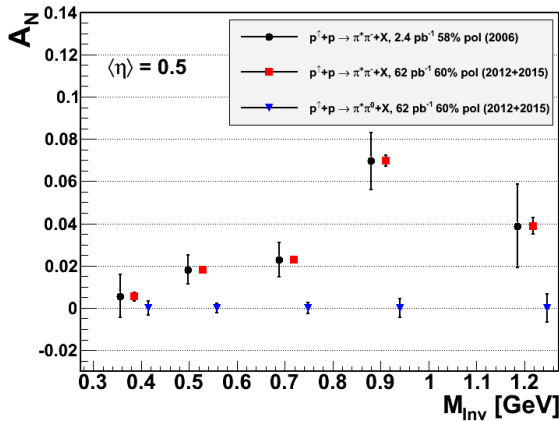


**Figure 4.5-2:** Runs 12 + 14 projections for the mid-rapidity Interference Fragmentation Function compared to the results based on Run 6.

Figure 4.5-2 shows the projected uncertainties for Run12+Run-14 for IFF for different pion combinations. The uncertainties for the Collins asymmetry as shown in Figure 4.2-8 will be reduced by a factor of 1.4 for Run 15 compared to Run 12. These 2 Run 15 results together with the Run-12 data will provide a powerful data set for global fits to extract transversity and to further constrain the Collins and interference

fragmentation functions. The STAR data will be extremely crucial to constrain transversity at high  $x$  as currently there are absolutely no data available. Both data sets are very stringent test to models trying to explain the transverse physics phenomena in p+p and especially the cause of the big forward pion  $A_N$ .

## 4.6. Physics with transversely polarised p+A collisions

### 4.6.1. Unpolarised observables

Our quest to understand QCD processes in Cold Nuclear Matter (CNM) centers on the following fundamental questions:

- What are the dynamics of partons at very small and very large momentum fraction ( $x$ ) in nuclei, and at high gluon-density. What are the nonlinear evolution effects (i.e. saturation)?
- What are the pQCD mechanisms that cause energy loss of partons in CNM, and is this intimately related to transverse momentum broadening?
- What are the detailed hadronization mechanisms and time scales and how are they modified in the nuclear environment?

Various aspects of these questions are being attacked by numerous experiments and facilities around the world. Deep inelastic scattering on nuclei addresses many of these questions with results from HERMES at DESY [17,18], CLAS at JLab [19], and in the future at the JLab 12 GeV upgrade and eventually an Electron-Ion Collider [20]. This program is complemented with hadron-nucleus reactions in fixed target p+A experiments at Fermilab (E772, E886, and soon E906) [21] at the CERN-SPS.

Current measurements at RHIC of the suppression of single hadrons [22,23] and back-to-back di-hadron correlations [24] in d+Au collisions have been interpreted as strong hints that the saturation scale, and the onset of saturation effects are accessible at forward rapidities at RHIC [25]. At this point, though, these interpretations are not unique, for two main reasons.

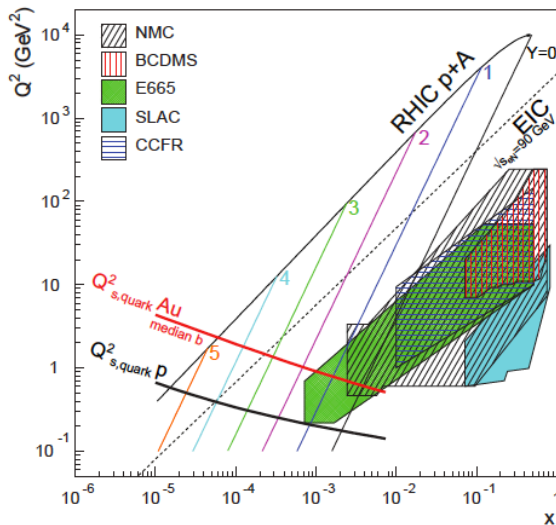


**Figure 4.6-1:** Kinematic coverage in the  $x$ - $Q^2$  plane for p+A collisions at RHIC, along with previous e+A measurements, the kinematic reach of an electron-ion collider (EIC), and estimates for the saturation scale  $Q_s$  in Au nuclei and protons. Lines are illustrative of the range in  $x$  and  $Q^2$  covered with hadrons at various rapidities.

First, as shown in Figure 4.6-1, for the kinematic reach of RHIC energies the saturation scale is moderate, on the order of a few  $\text{GeV}^2$ , so

measurements sensitive to the saturation scale are by necessity limited to semi-hard processes, and effects due to kinematic limits must be fully addressed. To some level this can be addressed at the LHC, where the larger energies allow for measurements deeper into the saturation regime, especially at forward rapidities. First measurements have been made at mid-rapidity by ALICE [26], which correspond approximately to  $y=3-4$  at RHIC. This measurement shows no suppression of single hadrons for  $p_T > 2$  GeV/c, as predicted by saturation models [27,28], however, alternative models also predict this feature of the data [29]. Key tests at the LHC will come at more forward rapidities, where saturation effects are expected to be stronger and distinct from other descriptions [28,29].

Second, and more importantly, in measurements to date in p+A collisions both the entrance and exit channels have components that interact strongly, leading to severe complications in the theoretical treatment. In p+A collisions, these complications can be ameliorated by removing the strong interaction from the final state, using photons and Drell-Yan electrons. Beyond this, the possibility of using polarized protons at RHIC to probe saturation phenomena is just beginning to be explored [30], utilizing the large transverse single-spin asymmetries seen in p+p collisions at forward rapidity (which do not require a polarized ion beam) to explore the onset of saturation.

Observables sensitive to parton saturation: Till today the golden channel at RHIC to observe strong hints of saturation are di-hadron correlations. The STAR di-hadron correlation results from Run 8 are shown in Figure 4.6-2, it shows the (efficiency uncorrected) probability to find an associated  $\pi^0$  given a trigger  $\pi^0$ , both in the forward region covered by STAR's Forward Meson Spectrometer (FMS). Shown is the coincidence signal versus azimuthal angle difference between the two pions in p+p collisions (left) compared to peripheral (center) and central d+Au collisions (right) [31]. The trigger and associated  $p_T$  ranges are indicated in the figure. All the distributions present two signal components, surmounting a constant background representing the underlying event contribution (larger in d+Au). The near-side peak represents the contribution from pairs of pions belonging to the same jet. It is not expected to be affected by saturation effects, therefore it is a useful tool to check the effective amount of broadening in the away-side peak. This away-side peak represents the back-to-back contribution to the coincidence probability, which should disappear in going from p+p to d+Au if saturation sets in. The data show that the width of the near-side peak remains nearly unchanged from p+p to d+Au, and particularly from peripheral to central d+Au collisions. Central d+Au collisions show a substantially reduced away side peak that is significantly broadened. Shown in the right plot of Figure 4.6-2 is a comparison with theoretical expectations using the CGC framework. The calculation uses a fixed saturation scale  $Q_s$  and considers valence quarks in the deuteron scattering off low-x gluons in the nucleus with impact parameter  $b = 0$  [32,33].

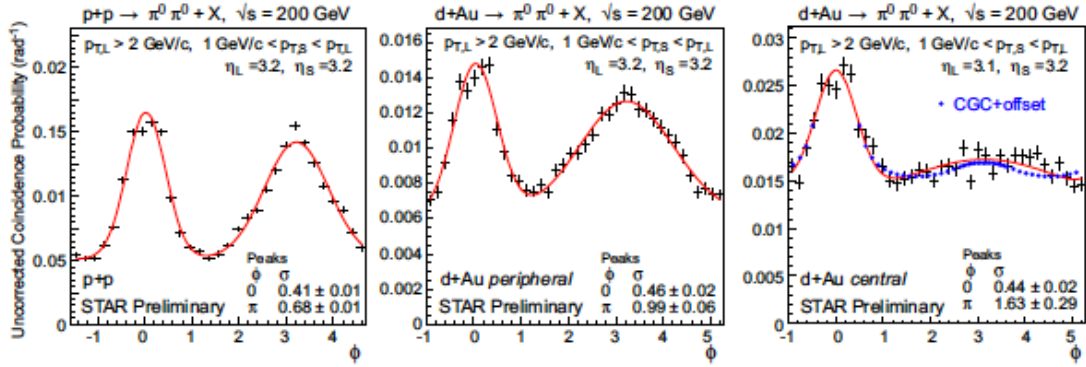


**Figure 4.6-2:** Uncorrected coincidence signal versus azimuthal angle difference between two forward neutral pions in p+p collisions (left) compared to peripheral (center) and central d+Au collisions (right) [31]. Data are shown with statistical errors and fit with a constant plus two Gaussian functions (in red). CGC expectations [32,33] have been superimposed (in blue) on the data for central d+Au collisions.

These data have been obtained from a sampled luminosity of  $44 \text{ nb}^{-1}$ . For an upcoming p+Au Run at RHIC the projection is  $175 \text{ nb}^{-1}/\text{week}$  after startup of the machine assuming a data taking efficiency of 70% and a run length of 5 weeks STAR could record  $300 \text{ nb}^{-1}$ . This would give the unique opportunity to vary the trigger and associated particle  $p_t$  from low to high values and such crossing the saturation boundary as shown in Figure 4.6-1 and reinstall the correlations for central p+A collisions for forward-forward  $\pi^0$ 's (see Figure 4.6-2 right plot). At forward rapidities  $\eta > 3$  the inclusive  $\pi^0$  cross section falls with  $1/p_T^6$  such to obtain the same statistical accuracy for  $p_T^{\text{trig}} > 3 \text{ GeV}$  a factor 11 in recorded luminosity would be needed. The requested  $300 \text{ nb}^{-1}$  would give a factor of 6 increase in sampled luminosity, this together with the improved performance of the FMS and the STAR triggering this should make it possible to study the di-hadron correlations also at higher  $p_T$ .

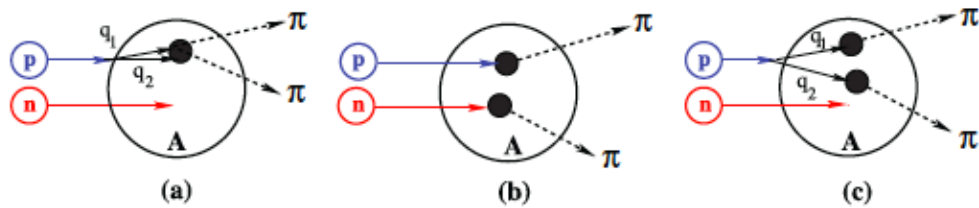


**Figure 4.6-3:** Contributions to two-pion production in d+A collisions through the double-interaction mechanism [34].

Studying di-hadron correlations in p+A collisions instead of d+A collisions has also the advantage that certain alternative interpretations can be ruled out. In reference [34], the authors point out that the contributions from double-parton interactions to the cross sections for  $d+A \rightarrow \pi^0 \pi^0 X$  are not negligible. This mechanism is illustrated in Figure 4.6-3. They find that such contributions become important at large forward rapidities, and especially in the case for d+A scattering. Whether or not this mechanism provides an alternative explanation of the suppression of the away-side peak in  $\pi^0$ - $\pi^0$  is not settled. However, this new insight provides a strong argument for performing the

proposed correlation studies in p+A, and not in d+A collisions. In addition, p+A collisions will facilitate cleaner centrality selections than possible in d+A, thus improving studies of the impact parameter dependence of nuclear and saturation effects.

The higher luminosity in the upcoming 2015 p+A run will also enable to study more luminosity hungry processes, i.e. direct photon, photon – jet, photon - hadron correlations.

**Cold nuclear effect on open heavy flavor and heavy quarkonia production:** The observations of large suppression of high  $p_T$  non-photon electron production [35] have led to concerted efforts in developing novel energy loss mechanism other than gluon radiations. Compared to the  $\pi^0$   $R_{AA}$  measurement, which is about the same at  $p_T > 1$  GeV/c, the non-photon electron  $R_{AA}$  gradually goes down from  $R_{AA} 1.0$  at  $p_T = 1$  GeV/c to  $R_{AA} 0.3$  at high  $p_T$ . The cold nuclear matter effects is believed to be the cause of the difference since large enhancement of non-photon electron production is observed in d+Au collisions [35,36]. Furthermore, the  $R_{AA}$  measurements of directly reconstructed  $D^0$  mesons shows an interesting bump at  $p_T = 2$  GeV/c [37], which may be due to the radial flow of light quarks that coalesce with charm quarks and the strong charm quark medium interaction during the medium evolution. However, the cold nuclear matter effect observed in non-photon electron measurements may also contribute to the formation of this interesting structure. It is therefore important for understanding the charm quark medium interaction to measure D meson production in p+Au collisions. The goal of  $D^0$  measurement in p+Au collisions is to reach similar precision as in p+p measurements as show in the right panel of Figure 3.3-4. For low  $p_T$  measurements, we will need 200M minimum bias events in  $|Vz| < 5$ cm. For high  $p_T$  measurements, we will need  $100 \text{ nb}^{-1}$  in  $|Vz| < 30$ cm sampled by HT0 ( $E_T > 2.6$  GeV) trigger.

The cold nuclear matter effects on heavy quarkonia production are critical in understanding the hot and dense medium effect of heavy quarkonia production in Au+Au collisions. It has long been a hot topic for discussion [38]. With the newly installed MTD, STAR will be able to sample the full luminosity with the di-muon trigger leading to high precision measurements of  $J/\psi \rightarrow \mu^+ \mu^-$  at low  $p_T$ . For  $p_T = 0 - 4$  GeV/c, the statistical uncertainty of the  $J/\psi \rightarrow \mu^+ \mu^-$   $R_{AA}$  measurements will be about 10% with  $300 \text{ nb}^{-1}$  p+Au collisions and  $90 \text{ pb}^{-1}$  p+p collisions sampled by di-muon trigger. For  $p_T = 4 - 8$  GeV/c, the statistical uncertainty of the  $J/\psi \rightarrow e^+ e^-$   $R_{AA}$  measurements will be about 5% with  $50 \text{ nb}^{-1}$  p+Au collisions and  $10 \text{ pb}^{-1}$  p+p collision sampled by HT1 ( $E_T > 3.5$  GeV) trigger in  $|Vz| < 30$ cm. For  $p_T = 8 - 10$  GeV/c, the statistical uncertainty of the  $J/\psi \rightarrow e^+ e^-$   $R_{AA}$  measurements will be about 15% with  $300 \text{ nb}^{-1}$  p+Au collisions and  $90 \text{ pb}^{-1}$  p+p collision sampled by HT2 ( $E_T > 5.4$  GeV) trigger.

**The ridge in p+A and d+A collisions at RHIC:** In p+Pb collisions at the LHC, an unambiguous two-particle correlation is observed at large pseudorapidity  $\Delta\eta$  and small azimuthal difference  $\Delta\phi$ . This is conventionally called the ridge. There are two leading theoretical explanations. One is the color glass condensate where small-x gluons are saturated below the saturation scale of  $Q_s$  in transverse momentum. At transverse

momentum  $\sim Q_s$ , two-gluon production is enhanced at small  $\Delta\phi$  over a large range in  $\Delta\eta$ . The other is hydrodynamic expansion in response to initial interaction geometry fluctuations. The anisotropy in final-state azimuthal distribution can be as large as 10% to explain the LHC ridge observation.

The two physics mechanisms likely give different predictions to the collision energy dependence of the ridge. It is therefore important to measure the ridge or the lack thereof at RHIC energies. STAR has analyzed the Run-3 d+Au data of approximately 10 million minimum bias events. The left plot below shows the 2D correlation function in  $(\Delta\eta, \Delta\phi)$  in top 20% central d+Au collisions for trigger and associated particle  $p_T$  ranges of  $0.15 < p_T^{\text{trig}} < 3$  GeV/c and  $1 < p_T^{\text{assoc}} < 2$  GeV/c, respectively. The right plot shows the  $\Delta\eta$  projections of the correlation function on the near side (red points) and away side (blue points). The correlation function is first subtracted by background determined by the ZYAM procedure. The large  $\Delta\eta$  tail of the near-side projection (the fit parameter C in the plot), which corresponds to the ridge, is presently consistent with zero with  $1\sigma$  of statistical error.

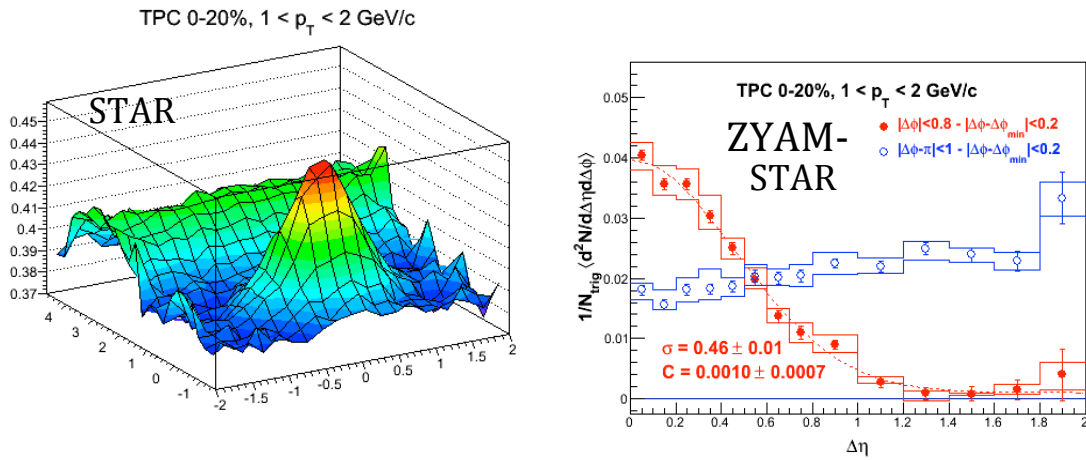


**Figure 4.6-4:** (Left plot) Au+Au, 0-20% in TPC multiplicity,  $0.15 < p_T^{\text{trig}} < 3$  GeV/c,  $1 < p_T^{\text{assoc}} < 2$  GeV/c. (Right plot) Au+Au, 0-20% in TPC multiplicity,  $0.15 < p_T^{\text{trig}} < 3$  GeV/c,  $1 < p_T^{\text{assoc}} < 2$  GeV/c.

In terms of anisotropic flow in the hydrodynamic picture, the data (the fit parameter C) can be converted into a  $v_2$  parameter value:  $C = 4v_2^2 \times \frac{1}{1.6} \int_{-0.8}^{0.8} \cos 2\Delta\phi d\Delta\phi = 2.5v_2^2$ . The data, taken as face value, correspond to a  $v_2$  value of  $3 \pm 3\%$ . If the central value stays at 3%, a  $5\sigma$  measurement would require 0.6% error. If the central value is zero, a 0.6% measurement would correspond to an upper limit of 1% at  $\sim 95\%$  confidence level. In order to make a 0.6% measurement, one would need about 25 times more statistics than the present 10M events, i.e. 250M minimum bias d+Au events. The data shown above are for top 20% centrality in TPC multiplicity. For a measurement of 0.6% absolute  $v_2$

error in top 5% d+Au, one would need 1 billion minimum bias events. The current data use an inclusive  $p_T$  range for the trigger particle. One would like to make more exclusive selection in trigger and associated  $p_T$ , such as 1-2 GeV/c for both. A rough estimate indicates  $\times 10$  more events are needed. Assuming p+A and d+A are similar in terms of the ridge correlation strength (perhaps with a factor of 2 difference), a data sample of 20 billion minimum bias p+A events would yield a solid measurement of the ridge. Taking p+Au total cross-section of 2 b, this would correspond to an integrated luminosity of  $10 \text{ nb}^{-1}$ .

**Cronin effect and strangeness enhancement in small-size systems:** The reason for requesting p+Au collisions is to study the particle type dependence of the Cronin effect, and strangeness enhancement in small-size systems. From experiences in Run 8 d+Au collisions, the study of particle type dependence of the Cronin effect at intermediate  $p_T$  requires more statistics compared to that to study the strangeness enhancement. Therefore we estimate the required statistics based on the measured  $R_{dAu}$  from Run 8 d+Au 200 GeV collisions. The collected statistics in Run 8 is about 70M minimum bias events. After the event selection 30M events remain.

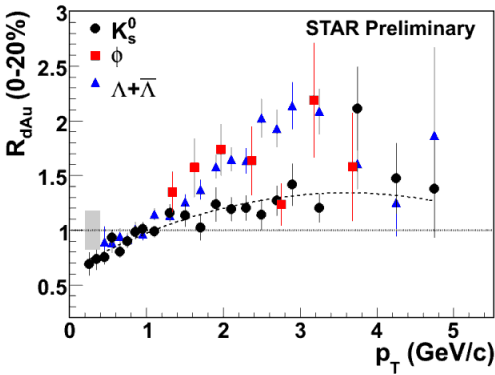


**Figure 4.6-5:**  $R_{dAu}$  for  $K_S^0$ ,  $\phi$  mesons and  $\Lambda$  hyperons in 0-20% d+Au central collisions from Run 8.

In the light flavor physics working group, one key study is to see whether there is a particle species dependence or baryon-meson dependence of the Cronin effect by comparing the  $R_{dAu}$  of  $\phi$  meson with other hadrons. The measured  $R_{dAu}$  for  $K_S^0$ ,  $\phi$  mesons and  $\Lambda$  hyperons in 0-20% central collisions from Run 8 is shown in Figure 4.6-5. One can see a clear separation between  $K_S^0$  and  $\Lambda$  hyperons at intermediate  $p_T$ . But for  $\phi$  mesons the result is not as clear. The large uncertainties for the  $\phi$  meson  $R_{dAu}$  are mainly due to a poor p+p reference sample (only 6.5M p+p non-single diffractive events from the year 2002 have been used). The uncertainties for the p+p reference could be controlled within  $\sim 5\%$  at intermediate  $p_T$  (2-4 GeV/c) with about 0.5B events from Run 9 and Run 12. If we assume  $\phi$  mesons  $R_{dAu}$  is close to  $\Lambda$  hyperons at around 3 GeV/c,  $R_{dAu}(\phi)/R_{dAu}(K_S^0)$  should be about 1.6. Considering that the ratio  $R_{dAu}(\phi)/R_{dAu}(K_S^0)$  should decrease with the number of participant nucleons, the  $R_{dAu}(\phi)/R_{dAu}(K_S^0)$  ratio should be about 1.3 in p+Au collisions at the same centrality. To have a 3-sigma significance, we need to control the relative uncertainty on  $R_{dAu}(\phi)/R_{dAu}(K_S^0)$  within 10% at  $p_T$  around 3 GeV/c. In Run 8 d+Au 0-20% centrality, the relative uncertainty on  $\phi$  meson raw yields at 3-3.5 GeV/c is about 8.3%. We need to control the error bar within 6% to make the uncertainty of  $R_{dAu}(\phi)/R_{dAu}(K_S^0)$  within 10%. Therefore, a factor of 2 more statistics is needed compared to Run 8 d+Au collisions. Considering that  $\phi$  meson yields in p+Au collisions are about a half of those in d+Au collisions, we need about  $7022 = 280\text{M}$  minimum bias p+Au events to make a good measurement.

#### 4.6.2. Polarised observables

**Single Transverse Spin Asymmetry in Polarized Proton-Nucleus Collisions:** As a result of exciting recent theoretical developments, the scattering of a polarized proton on an unpolarized nuclear target appears to have the potential to extend and deepen our understanding of QCD. In the frame where the nucleus is relativistic, its wave function consists of densely packed quarks and gluons, which constantly split and merge with each other. At high enough energies the density of the gluons is so high that the saturation regime is reached, characterized by strong gluon fields and scattering cross sections close to the unitarity bound. The saturated wave function is often referred to as the Color Glass Condensate (CGC) and is reviewed in detail in [39-43].

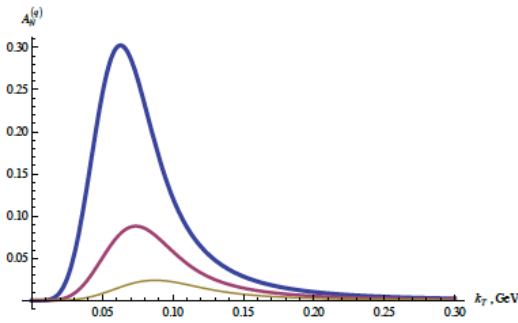


**Figure 4.6-6:** Quark SSA from Eq. (81) in [14] plotted as a function of  $k_T$  for different values of the target radius:  $R = 1$  fm (blue curve),  $R = 1.4$  fm (red curve), and  $R = 2$  fm (gold curve) for  $\alpha = 0.7$ .

Scattering a polarized probe on this saturated nuclear wave function may provide a unique way of probing the gluon and quark transverse momentum distributions (TMDs). In particular, the single transverse spin asymmetry  $A_N$  may provide access to the elusive nuclear Weizsaecker-Williams (WW) gluon distribution function [44,45], which is a solid prediction of the CGC formalism [46,47] but is very difficult to measure experimentally. The nuclear effects on  $A_N$  may shed important light on the strong interaction dynamics in nuclear collisions. While the theoretical approaches based on CGC physics predict that hadronic  $A_N$  should decrease with increasing size of the nuclear target [48-52] (see Figure 4.6-6), some approaches based on perturbative QCD factorization predict that  $A_N$  would stay approximately the same for all nuclear targets [53]. The asymmetry  $A_N$  for prompt photons is also important to measure. The contribution to the photon  $A_N$  from the Sivers effect [54] is expected to be non-zero, while the contributions of the Collins effect [55] and of the CGC-specific odderon-mediated contributions [14] to the photon  $A_N$  are expected to be suppressed [52,56]. Clearly experimental data on polarized proton-nucleus collisions is desperately needed in order to distinguish different mechanisms for generating the single spin asymmetry  $A_N$  in nuclear and hadronic collisions.

Figure 4.6-7 clearly shows that the requested statistics of  $40 \text{ pb}^{-1}$  and  $300 \text{ nb}^{-1}$  for p+p and p+Au, respectively, are sufficient to measure transverse spin observables in pA. The curves represent the theoretical prediction [51] for the suppression of SSA in the nuclear medium. This measurement will not only allow to get a handle on the saturation scale, but will also help to understand the underlying sub-process leading the big forward SSA in transverse polarized p+p. To distinguish further between the different theoretical models predicting a suppression of  $A_N$  in p+A, it will be also essential to measure  $A_N$  for direct photons. More details about the pre-shower in front of the FMS

and its performance as well as the capabilities to measure  $A_N$  for direct photons can be found in section 4.5.

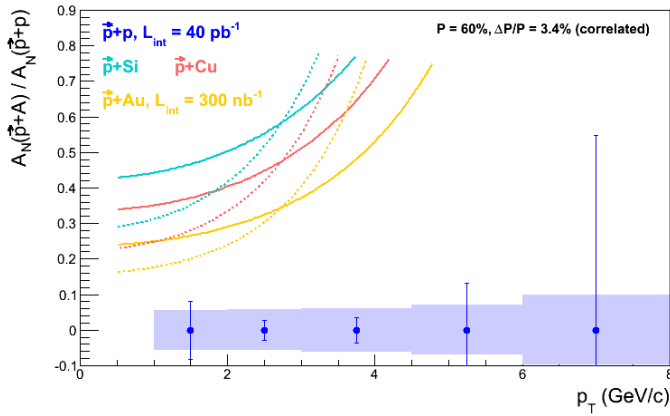


**Figure 4.6-7:** The projected statistical and systematic uncertainties for the ratio of  $A_N^{pA}/A_N^{pp}$  measured for  $\pi^0$ 's in the STAR FMS for the requested transverse p+p and p+A running. The colored curves follow Eq. 17 in Ref. [51] assuming  $Q_s^p = 1$  GeV (solid) and  $Q_s^p = 0.5$  GeV (dotted) with  $Q_s^A = A^{1/3} Q_s^p$ .

**Access to the generalized parton distribution  $E_g$ :** “How are the quarks and gluons, and their spins distributed in space and momentum inside the nucleon? What is the role of orbital motion of sea quarks and gluons in building the nucleon spin?” These are key questions, which need to be answered to understand overall nucleon properties like the spin structure of the proton. The formalism of generalized parton distributions (GPDs) provide till today the only theoretical framework, which allows some answers to the above questions [57]. The experimentally best way to constrain GPDs is through exclusive reactions in DIS, i.e., deeply virtual Compton scattering. RHIC with its possibility to collide transversely polarized protons with heavy nuclei has world-wide the unique opportunity to measure  $A_N$  for exclusive  $J/\psi$  in ultra-peripheral  $p^\uparrow$ +Au collisions (UPC) [58]. A non-zero asymmetry would be the first signature of a non-zero GPD  $E$  for gluons, which is sensitive to spin-orbit correlations and is intimately connected with the orbital angular momentum carried by partons in the nucleon and thus with the proton spin puzzle. To measure  $A_N$  for exclusive  $J/\psi$  in ultra-peripheral  $p^\uparrow$ +Au collisions provides an advantage in rate as the emission of the virtual photon from the gold nucleus is enhanced by  $Z^2$  compared to ultra-peripheral  $p^\uparrow$ +p collisions. Detecting the scattered polarized proton in “Roman Pots” and vetoing the break-up of the gold nucleus can ensure exclusivity of the process. The event generator SATRE [59], which also describes well the STAR results for  $r^0$  results for UPC in AuAu collisions, has been used to simulate exclusive  $J/\psi$  -production in  $p^\uparrow$ +Au UPC (see Figure 4.6-8 for the two contributing processes).

To select the  $J/\psi$  with the photon generated from the Au-beam cuts in the RP as installed for PHASE-II\* need to be applied, at 200 GeV the RP PHASE-II\* system has a  $t$ -acceptance from  $-0.016$   $\text{GeV}^2$  to  $-0.2$   $\text{GeV}^2$ . Figure 4.6-9 shows the generated  $t$ -spectra for the beam generating the photon (left) and the target beam (right). Requiring no hit in the RP phasing the Au-beam ( $t > -0.016$ ) or in the ZDC and a hit in the RP phasing the proton beam ( $-0.016 > t > 0.2$ ) together with the  $J/\psi$  decay electrons in the BEMC results in 250 exclusive  $J/\psi$ 's for a recorded luminosity of  $300$   $\text{nb}^{-1}$ , which is enough to have a look to the  $A_N$  in one bin for  $t$ . This statistics can be increased by also using the muons of the  $J/\psi$  decay detected in the MTD. Current studies using rapidity

gap triggers to tag diffraction and/or exclusive  $J/\psi$  production will show the statistics can be further increased.

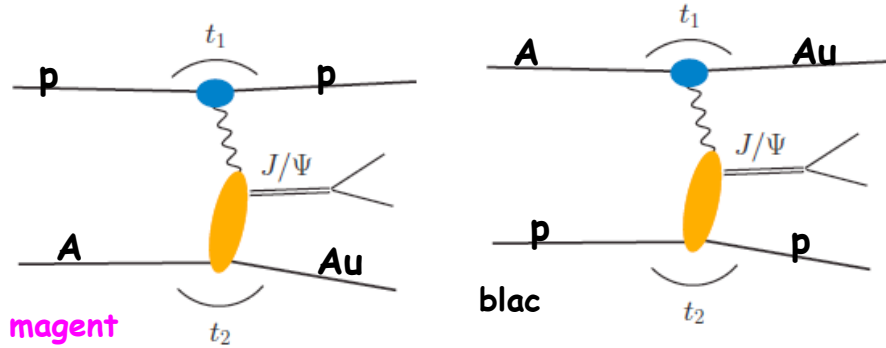


**Figure 4.6-8:** Possible processes to generate exclusive  $J/\psi$  in  $p^\dagger$ +Au UPC in one case the photon is generated by the proton beam (left) in the other by the gold beam (right).

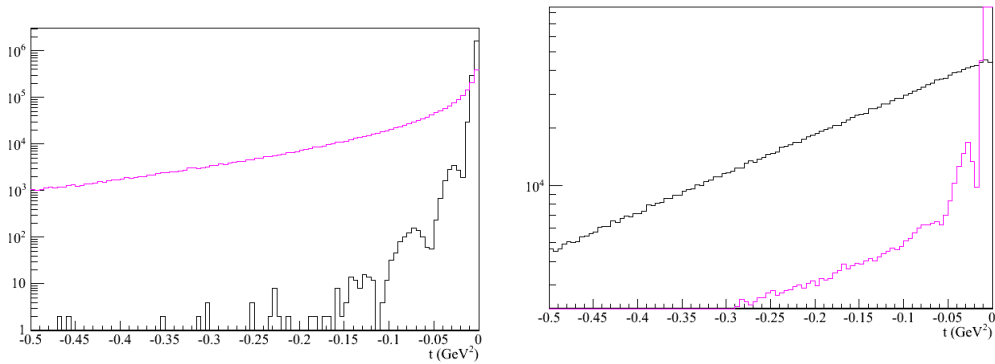


**Figure 4.6-9:** Generated  $t$ -spectra for the beam generating the photon (left) and the target beam (right) using the SATRE MC generator.

## References:

- [1] M. Aggarwal *et al.* (STAR Collaboration), Phys. Rev. Lett. **106**, 062002 (2011), arXiv: 1009.0326 [hep-ex].
- [2] A. Agakishiev *et al.* (STAR Collaboration), accepted for publication in Phys. Rev. D, arXiv:1112.2980 [hep-ex].
- [3] K. Melnikov and F. Petriello, Phys. Rev. D **74**, 114017 (2006), arXiv:hep-ph/0609070.
- [4] A. Martin, W. Stirling, R. Thorne, and G. Watt, Eur. Phys. J. **C63**, 189 (2009), arXiv: 0901.0002 [hep-ph].
- [5] B. I. Abelev *et al.* (STAR Collaboration), Phys. Rev. Lett. **101**, 222001 (2008), arXiv: 0801.2990 [hep-ex].
- [6] K. Kanazawa and Y. Koike, Phys. Rev. D **83**, 114024 (2011).
- [7] D. de Florian, R. Sassot, M. Stratmann, and W. Vogelsang, Phys. Rev. Lett. **101**, 072001 (2008) and Phys. Rev. D **80**, 034040 (2009).

- [8] E.A. Hawker *et al.*, Phys. Rev. Lett. **80**, 3715 (1998); R.S. Towell *et al.*, Phys. Rev. D **64**, 052002 (2001).
- [9] D. de Florian, R. Sassot, M. Stratmann, and W. Vogelsang, Phys. Rev. Lett. **101**, 072001 (2008); Phys. Rev. D **80**, 034030 (2009).
- [10] M.M. Aggarwal *et al.*, Phys. Rev. Lett. **106**, 062002 (2011).
- [11] P. Djawotho *et al.*, arXiv:1106.5769.
- [12] L. Adamczyk *et al.* arXiv:1205.2735.
- [13] D. de Florian, R. Sassot, M. Stratmann, and W. Vogelsang, Prog. Nucl. Part. Phys. **67**, 251 (2012).
- [14] M. Walker *et al.*, arXiv:1107.0917.
- [15] B.I. Abelev *et al.*, Phys. Rev. Lett. **100**, 232003 (2008).
- [16] L. Gamberg and Z.-B. Kang, Phys.Lett. B718 (2012) 181-188
- [17] HERMES Collaboration, A. Airapetian *et al.*, Phys. Lett. B684:114–118, 2010. arXiv:0906.2478
- [18] HERMES Collaboration, A. Airapetian *et al.*, Phys. Lett., B577:37–46, 2003. arXiv:hep-ex/0307023,
- [19] W. Brooks, Physics with nuclei at an Electron Ion Collider. 2010. arXiv:1008.0131.
- [20] W. Brooks and H. Hakobyan, Nucl. Phys, A830:361c–368c, 2009. arXiv:0907.4606
- [21] E866 Collaboration, M. Vasilev *et al.*, Phys. Rev. Lett., 83:2304–2307, 1999. arXiv:hep-ex/9906010
- [22] BRAHMS Collaboration, I. Arsene *et al.*, Phys.Rev.Lett. 93, 242303 (2004), nucl-ex/0403005.
- [23] STAR Collaboration, J. Adams *et al.*, Phys.Rev.Lett. 97, 152302 (2006), nucl-ex/0602011.
- [24] PHENIX Collaboration, A. Adare *et al.*, Phys.Rev.Lett. 107, 172301 (2011), 1105.5112.
- [25] J. L. Albacete and C. Marquet, Phys.Rev.Lett. 105, 162301 (2010), 1005.4065.
- [26] ALICE Collaboration, B. Abelev *et al.*, (2012), 1210.4520.
- [27] P. Tribedy and R. Venugopalan, Phys.Lett. B710, 125 (2012), 1112.2445.
- [28] J. L. Albacete, A. Dumitru, H. Fujii, and Y. Nara, (2012), 1209.2001.
- [29] I. Helenius, K. J. Eskola, H. Honkanen, and C. A. Salgado, (2012), 1207.6869.
- [30] Z.-B. Kang and F. Yuan, Phys.Rev. D84, 034019 (2011), 1106.1375.
- [31] E. Braidot for the STAR Collaboration, arXiv:1008.3989 [nucl-ex].
- [32] C. Marquet, Nucl. Phys. A 796, 41 (2007) [arXiv:0708.0231 [hep-ph]].
- [33] J. L. Albacete and C. Marquet, arXiv:1005.4065 [hep-ph].
- [34] M. Strikman and W. Vogelsang, arXiv:1009.6123 [hep-ph].
- [35] S. S. Adler *et al.* (PHENIX Collaboration), Phys. Rev. Lett. 96, 032301 (2006); B.I. Abelev *et al.* (STAR Collaboration), Phys. Rev. Lett. 98, 192301 (2007); B. I. Abelev *et al.* (STAR Collaboration), Phys. Rev. Lett. 106, 159902(E) (2011).
- [36] A. Adare *et al.* (PHENIX Collaboration), Phys Rev. Lett. 109, 242301 (2012).
- [37] Y.F. Zhang (for STAR Collaboration), QM 2011 proceedings; D. Tlusty (for STAR Collaboration), QM 2012 proceedings.
- [38] A. Adare *et al.* (PHENIX Collaboration) Phys. Rev. Lett. 107, 142301 (2011); B. Trzeciak for STAR Collaboration, QM 2012 proceedings; M. Wysocki for PHENIX Collaboration, QM 2012 proceedings.

- [39] H. Weigert, Prog. Part. Nucl. Phys. **55** (2005) 461.
- [40] E. Iancu and R. Venugopalan, hep-ph/0303204.
- [41] F. Gelis, E. Iancu, J. Jalilian-Marian, and R. Venugopalan, Ann. Rev. Nucl. Part. Sci. **60** (2010) 463.
- [42] Y. V. Kovchegov and E. Levin, Quantum Chromodynamics at High Energy. Cambridge University Press, 2012.
- [43] J. Jalilian-Marian and Y. V. Kovchegov, Prog. Part. Nucl. Phys. **56** (2006) 104.
- [44] A. Metz and J. Zhou, Phys. Rev. D **84** (2011) 051503.
- [45] F. Dominguez, J.-W. Qiu, B.-W. Xiao, and F. Yuan, Phys. Rev. D **85** (2012) 045003; J. Jalilian-Marian, A. Kovner, L. D. McLerran, and H. Weigert, Phys. Rev. D **55** (1997) 5414.
- [46] Y. V. Kovchegov and A. H. Mueller, Nucl. Phys. **B529** (1998) 451.
- [47] F. Dominguez, C. Marquet, B.-W. Xiao, and F. Yuan, Phys. Rev. D **83** (2011) 105005.
- [48] D. Boer, A. Dumitru, and A. Hayashigaki, Phys. Rev. D **74** (2006) 074018.
- [49] D. Boer and A. Dumitru, Phys. Lett. **B556** (2003) 33.
- [50] D. Boer, A. Utermann, and E. Wessels, Phys. Lett. **B671** (2009) 91.
- [51] Z.-B. Kang and F. Yuan, Phys. Rev. D **84** (2011) 034019.
- [52] Y. V. Kovchegov and M. D. Sievert, Phys. Rev. D **86** (2012) 034028.
- [53] J.-W. Qiu, talk at the workshop on “Forward Physics at RHIC”, RIKEN BNL Research Center, BNL, 2012.
- [54] D. W. Sivers, Phys. Rev. D **41** (1990) 83.
- [55] J. C. Collins, Phys. Lett. **B536** (2002) 43.
- [56] L. Gamberg and Z.-B. Kang, arXiv:1208.1962.
- [57] D. Mueller, Fortschr. Phys. **42** (1994) 171; X.-D. Ji, Phys. Rev. Lett. **78**, 610 (1997); J. Phys. **G24** (1998) 1181; K. Kumericki, D. Mueller, and K. Passek-Kumericki, Nucl. Phys. **B794** (2008) 244; K. Kumericki and D. Mueller, arXiv:1205.6967.
- [58] S. Klein and J. Nystrand, hep-ph/0310223.
- [59] T. Toll and T. Ullrich, Phys. Rev. C **87** (2013) 024913

## 5. Physics with Tagged Forward Protons at STAR

There are two main reactions that can be studied with tagged forward protons: polarized proton-proton elastic scattering and Central Exclusive Production (CEP) in double Pomeron exchange (DPE); see Figure 5-1. Since the proton beams at RHIC are polarized we will study the spin dependence of the diffractive process.

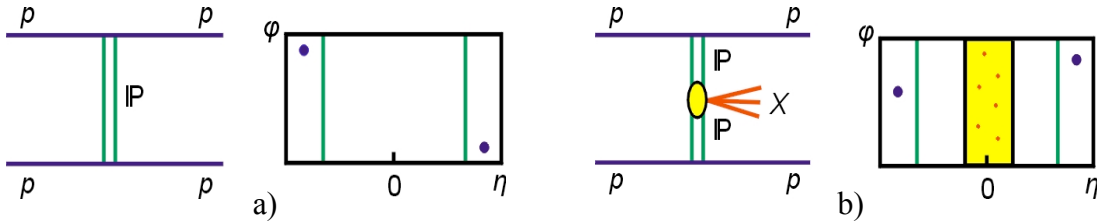


**Figure 5-1:** a) Elastic Scattering diagram, and b) Central Exclusive Production diagram. Feynman diagrams and corresponding azimuthal angle vs. pseudorapidity diagrams are also shown.

A process of unique interest at RHIC is the central production process through the DPE mechanism  $p+p \rightarrow pM_Xp$ , as shown in Figure 5-1b. The two protons stay intact after the interaction, but they lose momentum to the Pomeron and the Pomeron-Pomeron interaction produces a system  $M_X$  at mid-rapidity of the colliding protons.

The Roman Pot detectors used for the pp2pp experiment and STAR Run 9 [1-5] installed in the location of Phase-II\*, will be used to tag very forward protons, thus selecting processes in which the proton stays intact, as in Figure 5-1. The Central Production Process can be studied also in proton-nucleus (pA) collisions, where the trigger would be proton on one side and a rapidity gap on the other side.

### 5.1. Central exclusive production (CEP) in p+p collisions

Tagging and measuring the forward protons is important since it removes the ambiguity of a (complementary) rapidity gap tag, which has a background due to the low multiplicity of diffractive events. The momentum balance between the scattered protons and the centrally produced system, exclusivity condition, allows obtaining a relatively background free data sample, like the one obtained in Run 9 at  $\sqrt{s} = 200$  GeV, for which the statistics of the data sample was limited because of the luminosity and the  $t$ -range for that run.

In Figure 5.1- we show a preliminary measurement of the invariant mass spectrum of the  $\pi^+\pi^-$  pairs produced in the exclusive process  $p+p \rightarrow pM_Xp$  (CEP), obtained with the STAR detector at RHIC at  $\sqrt{s} = 200$  GeV in 4 days running during Run 9. The Roman Pots were used to tag forward protons and the invariant mass of the pion pair was

obtained using tracks reconstructed in the STAR Time Projection Chamber (TPC). To select CEP events the balance of momenta of the outgoing protons and central  $\pi^+\pi^-$  pair was required. These events can be seen in Figure 5.1-1 (left) as a diagonal band. The resulting distribution of invariant mass of the central pair for the selected CEP events is displayed in Figure 5.1-1 (right), which also shows a very small non-exclusive background estimated from events with like-sign charge pairs.

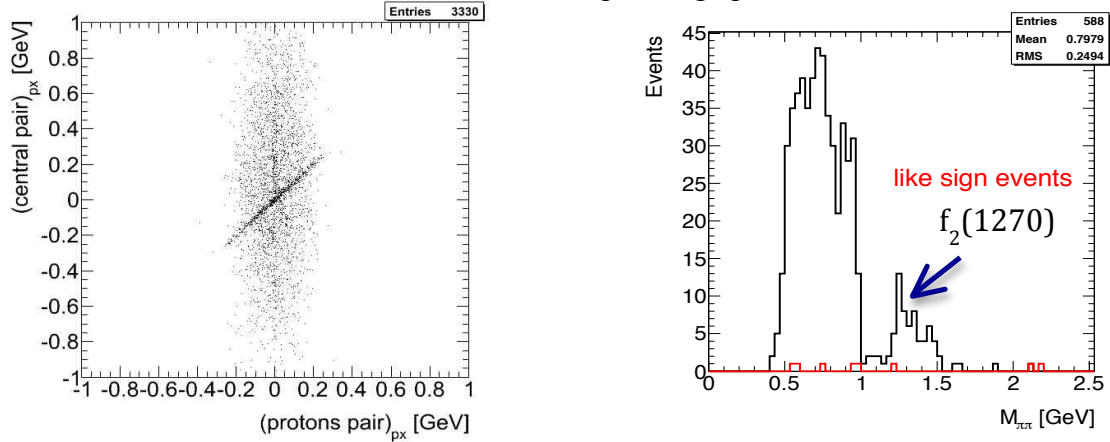


**Figure 5.1-1:** (left) Transverse momentum correlation of the  $\pi^+\pi^-$  pairs measured in the STAR TPC vs transverse momentum of proton pair measured in the Roman Pots; (right) Invariant mass of the  $\pi^+\pi^-$  pairs using the events in the correlation band, a small background of like sign  $\pi\pi$  pairs events, in red, is also shown.

One of the interesting physics topics that can be explored at RHIC is a glueball search in the Double Pomeron Exchange (DPE) process. Because of the constraints provided by the double Pomeron interaction, the glueballs, and other states coupling preferentially to gluons, are expected to be produced with much reduced backgrounds compared to standard hadronic production processes [6].

Two of the gluons in the DPE process, see Figure 5.1, could merge into a mesonic bound state without a constituent quark, a glueball in the central production  $p+p \rightarrow pM_Xp$ . The lattice QCD calculations predict the lowest-lying scalar glueball state will have a mass in the range 1500-1700  $\text{MeV}/c^2$ , with tensor and pseudoscalar glueballs in the range 2000-2500  $\text{MeV}/c^2$  [6].

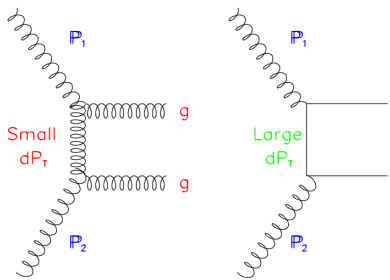


**Figure 5.1-2:** Schematic diagrams of the coupling of the exchanged particles into the final state meson for a) gluon exchange and b) quark exchange [6].

Experimentally measured candidates for the scalar glueball states are the  $f_0(1500)$  and the  $f_J(1710)$  in central production [7] as well as other gluon-rich reactions such as  $p \bar{p}$  annihilation, and radiative  $J/\psi$  decay [8]. The spin of the  $f_J(1710)$  is not yet confirmed, indications for both spin 2 and spin 0 have been reported. The glueballs are expected to

be intrinsically unstable and decay in diverse ways, yielding typically two or more mesons. The  $f_J(1710)$  dominantly decays into  $K^+K^-$  pairs, and  $f_0(1500)$  into  $\pi^+\pi^-\pi^+\pi^-$ .

With the Phase-II\* in Run 15 we expect to collect a data sample in a wider  $t$  range, allowing for much larger statistics as compared to that in Figure 5.1-2. Thus allowing a detailed study of the structure seen there.

Simulations indicate that during 5 weeks of p+p running in Run 15 ( $40 \text{ pb}^{-1}$ ) one can collect  $1 \times 10^6 K^+K^-$  and  $1.5 \times 10^6 \pi^+\pi^-\pi^+\pi^-$  data sample in  $1 < M_X < 2 \text{ GeV}/c^2$  for analysis, assuming branching ratios of DPE processes measured at  $\sqrt{s} = 62.4 \text{ GeV}$  [9]. The two Pomeron cross-section at RHIC energies is not known and an estimate of  $140 \text{ } \mu\text{barn}$  from Ref. [10] was used in our simulations.

## 5.2. Elastic scattering at medium $|t|$

Elastic p+p scattering is a paradigm in the study of the diffraction process at the highest available energies. The special role of the elastic channel, contributing about 20% of the total cross section, can be interpreted in terms of the optical theorem, as the shadow of many inelastic channels, open at high energies: in this respect the elastic amplitude is considered to be mainly imaginary and helicity-conserving. This is reflected in the phenomenological features of a simple Pomeron Regge-exchange, with vanishing spin-flip, which implies a decrease of polarization asymmetries as energy increases.

Almost the entire energy range of this proposal has been inaccessible to proton-proton scattering in the past. A measurement of the total cross section,  $\sigma_{\text{tot}}$  and spin dependence of the elastic scattering in the  $t$ -range  $[0.02, 0.12]$  will be studied.

## References

- [1] S. Bültmann et al., *Phys. Lett.* **B579** (2004) 245.
- [2] S. Bültmann et al., *Nucl. Instr. Meth.* **A535** (2004) 415.
- [3] S. Bültmann et al., *Phys. Lett.* **B632** (2006) 167.
- [4] S. Bültmann et al., *Phys. Lett.* **B647** (2007) 98.
- [5] W. Guryn et al., RHIC Proposal R7 (1994) (unpublished).
- [6] For a review, see F.E. Close, *Rep. Prog. Phys.* **51**, 833 (1988), and C. Amsler and N.A. Tornqvist, *Phys. Rept.* **389**, (2004) 61.
- [7] S. Abatziz et al., *Phys. Lett.* **B324**, (1994) 509.
- [8] V. Crede and C.A. Meyer, *Prog. Part. Nucl. Phys.* **63**, (2009) 74.
- [9] A. Breakstone et al., *Z. Phys.* **C42**, (1984) 387.
- [10] K.H. Streng, *Phys. Lett.* **B166**, (1986) 443.